Area Spectral Efficiency of Cellular Mobile Radio Systems

Mohamed-Slim Alouini, *Member, IEEE*, and Andrea J. Goldsmith, *Member, IEEE*

***Abstract*— A general analytical framework quantifying the spectral efficiency of cellular systems with variable-rate transmission is introduced. This efficiency, the area spectral efficiency, defines the sum of the maximum average data rates per unit bandwidth per unit area supported by a cell's base station. Expressions for this efficiency as a function of the reuse distance for the worst and best case interference configurations are derived. Moreover, Monte Carlo simulations are developed to estimate the value of this efficiency for average interference conditions. Both fully loaded and partially loaded cellular systems are investigated. The effect of random user location is taken into account, and the impact of lognormal shadowing and Nakagami multipath fading is also studied.**

***Index Terms*—Adaptive transmission systems, cellular systems capacity, cochannel interference, spectral efficiency.**

I. Introduction

THE RADIO spectrum available for wireless data services and systems is extremely scarce, while demand for these service is growing at a rapid pace [1]. Spectral efficiency is therefore of primary concern in the design of future wireless data communications systems. This efficiency is partly achieved by cellular systems which exploit the power falloff with distance of signal propagation to reuse the same frequency channel at spatially separated locations [2]. However, while frequency-reuse provides more efficient use of the limited available spectrum, it also introduces unavoidable cochannel interference [3]–[8], which ultimately determines the bit error rates (BER's) available to each user. Thus, there is a tradeoff between the *system* spectral efficiency, measured in [b/s]/[Hz $\cdot$ m^2] or Erlangs/[Hz $\cdot$ m^2], and the communication link quality, measured in terms of the BER provided to the users [5], [8].

Another technique to increase spectral efficiency is to use multilevel modulation, such as M-QAM, which increase *link* spectral efficiency, measured in [b/s]/Hz, by sending multiple bits per symbol [9]. However, wireless channels are subject to severe propagation impairment which results in a serious degradation in the link carrier-to-noise ratio (CNR), and even if efficient fading compensations techniques are used, multilevel schemes will still require higher power levels than binary modulations for a specified BER. Therefore, to keep the cochannel interference at an acceptable level it is necessary to increase the frequency-reuse distance (or equivalently the cluster size) which in turns leads eventually to a lower *system* efficiency. This problem has been recently addressed by Haas and Belfiore [10], who showed that there is a tradeoff between the system and link spectral efficiencies. This was also confirmed by Morinaga *et al.* [11], who claimed that 4-QAM is the optimum multilevel modulation for high-capacity cellular systems, and that opting for higher modulation levels will just reduce the system spectral efficiency. This is essentially due to the fact that fixed modulation systems are designed relative to the worst case interference/fading conditions. However, adapting certain parameters of the transmitted signal relative to the CNR leads to better link and system spectral efficiencies. The basic concept of variable-rate transmission is real-time balancing of the link budget through adaptive variation of the symbol time duration, constellation size, coding rate/scheme, or any combination of these parameters [12]–[16]. Thus, without wasting power, increasing cochannel interference, or sacrificing BER, these schemes provide a much higher average spectral efficiency by taking advantage of the "time-varying" nature of the wireless channel and interference conditions: transmitting at high speeds under favorable interference/channel conditions and responding to an increase in interference and/or channel degradation through a smooth reduction of their data throughput. Since buffering/delay of the input data may be required in this process, adaptive systems are to be used for applications which are, to some extent, bursty in nature and are therefore best suited to high-speed wireless data transmission.

Previous studies of the system spectral efficiency for cellular systems assumed that the data rate is constant and equal for all users, regardless of interference conditions and channel quality [4], [5], [8], [10], [17]–[19]. In these papers, spectral efficiency calculations was based on a criterion introduced by Hatfield [17] and defined as the ratio of the carried traffic per cell (in Erlangs) to the product of the total system bandwidth and area supported by a base station. This criterion is not suitable for data systems since Erlangs are just a measure of traffic loading rather than throughput intensity. A more pertinent

Manuscript received May 9, 1997; revised April 8, 1998. This work was supported in part by the NSF CAREER Development Award NCR-9501452 and by Pacific Bell. This is an expanded version of work which was presented at the IEEE Vehicular Technology Conference VTC'97, Phoenix, AZ, May 1997, and at the IEEE International Conference on Communications ICC'97, Montreal, P.Q., Canada, June 1997.

M.-S. Alouini was with the Communication Group, Department of Electrical Engineering, California Institute of Technology (Caltech), Pasadena, CA 91125 USA. He is now with the Department of Electrical and Computer Engineering, University of Minnesota, Minneapolis, MN 55455 USA (e-mail: alouini@ece.umn.edu).

A. J. Goldsmith was with the Communications Group, Department of Electrical Engineering, California Institute of Technology (Caltech), Pasadena, CA 91125 USA. She is now with the Department of Electrical Engineering, Stanford University, Stanford, CA 94305 USA (e-mail: andrea@ee.stanford.edu).

Publisher Item Identifier S 0018-9545(99)05742-4.

measure of spectral efficiency in cellular data systems is the total throughput, i.e., number of [b/s]/[Hz · m^2] associated with each base station (BS).

The aim of this paper is to investigate the theoretical limits of this spectral efficiency limits for cellular data systems where mobile users continuously adapt their rate relative to their fading and interference conditions. This efficiency, called the area spectral efficiency (ASE), is defined as the sum of the maximum average data rates per unit bandwidth per unit area for a specified BER. The ASE definition captures the tradeoffs between a cellular system' spectral efficiency, the users' link spectral efficiency, and the communication link quality provided to these users. We take into account the effect of the users random location in their respective cells and study the ASE under the impact of shadowing, and multipath fading superimposed on path loss, with propagation parameters for both macrocells and microcells. Although both shadowing and fading will typically be superimposed on path loss, we first consider these two phenomena separately to assess their respective impact. We then study their combined effect on the ASE. For our analyses and simulations, we regard only the uplink (mobile to BS) of systems using frequency-division multiple access (FDMA) or time-division multiple access (TDMA). We first consider fully loaded cellular systems. We then generalize our analysis to partially loaded systems, and determine the effect of traffic loading on the ASE.

The remainder of this paper is organized as follows. The next section describes in more detail our propagation, cochannel interference, adaptive transmission system, and user's random location models. Section III introduces the concept of ASE for fully loaded cellular systems. Section IV presents analyses, computer simulations, and numerical results for the ASE when only path loss is considered. The impact of shadowing and multipath fading on the ASE are studied in Section V and VI, respectively. Section VII considers the combined effect of shadowing and multipath fading on the ASE. Section VIII deals with the ASE of partially loaded systems. Finally, the paper concludes with a review of the main results.

II. Channel and System Models

In this section, we first outline the models for the different propagation impairments affecting cellular systems. We then present our assumptions for the cochannel interference and the adaptive communication system under consideration. We finally describe the random location model used for the users' positions.

A. Propagation Models

It is well known that signal propagation in a radio mobile environment is affected by three independent phenomena: 1) deterministic path-loss variation with distance; 2) random slow shadowing; and 3) random fast multipath fading.

Path loss is due to the decay of the intensity of a propagating radio-wave. In both our analyses and simulations, we use the *two-slope* path-loss model [20] to obtain the average received power as function of distance. According to this model, the average received signal power $\overline{S}$ [W] is given by

$$\overline{S} = \frac{K}{r^a\ (1+r/g)^b} S_t \tag{1}$$

where K is a constant, r [m] is the distance between the mobile and the BS, a is the basic path-loss exponent (approximately two), b is the additional path-loss exponent (ranges from two to six), and S_t [W] is the transmitted signal power. The parameter g [m] is called the *break point* of the path-loss curve and is given by $g = (4h_B h_m)/\lambda_c$, where h_B [m] is the BS antenna height, h_m [m] is the mobile antenna height, and λ_c [m] is the wavelength of the carrier frequency. We use the following typical values [21]: $h_m = 2$ m, $h_B = 10$ m for microcells and $h_B = 50$ m for macrocells. The resultant break points for 900-MHz systems are $g \simeq 240.3$ m for microcells, and $g \simeq 1212$ m for macrocells. For 2-GHz systems, the break points increase to $g \simeq 533$ m for microcells, and $g \simeq 2667$ m for macrocells.

In urban microcells systems, the link quality is also affected by the shadowing of the line-of-sight path from terrain, buildings, and trees. The shadowing is generally modeled as lognormal distributed [22, Sec. 2.4]. The probability density function (PDF) of the slowly varying received signal power is thus given by the standard lognormal expression

$$p_S(s) = \frac{\xi}{\sqrt{2\pi}\sigma s} \exp\left(-\frac{(\xi \ln(s) - \mu)^2}{2\sigma^2}\right), \qquad s \geq 0 \tag{2}$$

where $\xi = 10/\ln 10 = 4.3429$, $\mu = \xi \ln(\overline{S})$ is the area (logarithmic) mean power which is related to path loss and which is expressed in decibels (dB), and σ is the shadow (logarithmic) standard deviation in decibels.

Mobile radio systems are also subject to fast (relative to the shadowing effect) multipath fading due to the combination of randomly delayed reflected, scattered, and diffracted signal components. We consider slowly varying flat-fading multipath channels. The slowly varying condition holds when the channel fading changes at a rate much slower than the data rate, so the channel remains constant over hundreds of symbols. Flat fading occurs when the symbol time duration is much greater than the delay spread so the signal is just affected by a degradation in its strength without a distortion in its shape. We assume that the multipath fading environment is characterized by a Nakagami-m distribution such as the PDF of the amplitude of the received signal A is given by [23, eq. (11)]

$$p_A(a) = 2\left(\frac{m}{\Omega}\right)^m \frac{a^{2m-1}}{\Gamma(m)} \exp\left(-m\frac{a^2}{\Omega}\right), \qquad a \geq 0 \tag{3}$$

where $\Omega = E_S[S] = E_A[A^2]$ is the local mean received power which is related to path loss and shadowing, m is the Nakagami *fading parameter* ($m \geq 1/2$), and $\Gamma(.)$ is the *gamma function* defined by [24, p. 942, eq. (8.310.1)]

$$\Gamma(z) = \int_0^{+\infty} t^{z-1} e^{-t}\, dt, \qquad z \geq 0. \tag{4}$$

Thus, the PDF of the received signal power $S = A^2$ is a gamma distribution given by

$$p_S(s) = \left(\frac{m}{\Omega}\right)^m \frac{s^{m-1}}{\Gamma(m)} \exp\left(-m\frac{s}{\Omega}\right), \qquad s \geq 0. \quad (5)$$

The amount of fading of a channel AF is defined as the variance of the received power to the square of the mean of the received energy [25]. For the Nakagami-m distribution, $AF = 1/m$. The Nakagami-m distribution therefore spans a range of fading environments via the m parameter. For instance, it includes the one-sided Gaussian distribution ($m = 1/2$, which corresponds to worst case fading) and the Rayleigh distribution ($m = 1$) as special cases. In addition, when $m > 1$, a one-to-one mapping between the Rician K factor and the Nakagami m parameter allows the Nakagami-m distribution to closely approximate the Rice distribution [23]. As m increases, the fading amount AF decreases, and in the limit as $m \longrightarrow \infty$, $AF \longrightarrow 0$, and the Nakagami fading channel converges to an additive white Gaussian noise (AWGN) channel. Finally, and perhaps most importantly, the Nakagami distribution often gives the best fit to urban [26], [27] and indoor [28] multipath propagation.

Although path loss, shadowing, and multipath fading simultaneously affect a radio mobile communication link, we first analyze their effects separately to quantify their respective impact on the ASE. We then study their combined effect on the ASE in Section VII. This separation is valuable since in many cases lognormal or Nakagami distributions give the best fit for the overall fading process. For instance, Suzuki [26] concludes that the distribution of the path strengths within a site tends to follow a lognormal or a Nakagami distribution. In addition, Abbes and Sheikh [29] recently showed that both lognormal and Nakagami distributions fit the overall fading data for LOS microcells, and argued that the segregation of slow and fast fading components (e.g., lognormal and Nakagami) is therefore unnecessary.

B. Interference and the Adaptive System Models

To simplify the analyses the following assumptions have been made in the cochannel interference model. First, we consider interference-limited systems in which the thermal noise power is negligible relative to the cochannel interference power [18]. Thus, the ratio of carrier power to noise plus interference power reduces to the carrier-to-interference power ratio (CIR). We also neglect cochannel interferers outside the first dominant tier of interfering cells and all interchannel interference [18]. Therefore, the desired user CIR, γ_d, can be written as

$$\gamma_d(n_I) = \frac{S_d}{S_I} = \frac{S_d(r)}{\sum_{i=1}^{n_I} S_i(r_i)}, \qquad n_I = 1, \cdots, N_I \quad (6)$$

where S_d [W] is the received power level from the desired mobile at a distance r from its BS, S_I [W] is the total interfering power, and S_i [W] is the received power level from the ith interfering mobile at a distance r_i from the desired mobiles' BS. We assume throughout our study that the cochannel interfering signals add up incoherently since this leads to a more realistic assessment of the cochannel interference in cellular systems [5]. In (6), n_I is the number of active cochannel interferers in the first tier, and N_I is the maximum number for n_I. For example, $N_I = 6$ for nonsectorized cellular systems, whereas $N_I = 2$ for 120° cell sectorized systems or linear highway cellular systems. The interference model for the uplink of a fully loaded nonsectorized ($N_I = 6$) cellular system is shown in Fig. 1.

Since the signal powers of both the desired and interfering mobiles experience fluctuations due to multipath fading, shadowing, and the random location of users in their respective cells, γ_d is also a random variable which depends on the distribution of the S_d and S_is. Accurate techniques for "real-time" estimation of these variations in the CIR are available [30], and we assume throughout this paper that the fluctuations in the CIR γ_d are tracked perfectly by the BS receiver. We also assume that this information is sent back to the transmitting mobiles via an error-free feedback path. The time delay in this feedback path is also assumed to be negligible compared to the rate of the channel/interference variations. All these assumptions, which are reasonable slowly varying channels, allow the mobiles to adapt their transmission rate relative to the actual CIR state. A block diagram of the adaptive transmission system model is shown in Fig. 3.

C. Users' Random Location Model

For analytical convenience, we assume that the cell shape is approximated by a circle of radius R. All the mobiles (desired and interfering users) are assumed to be mutually independent and uniformly distributed in their respective cells. Thus, the PDF of the mobiles polar coordinates (r, θ) relative to their BS's are

$$p_r(r) = \frac{2\,(r - R_o)}{(R - R_o)^2}, \qquad R_o \leq r \leq R \quad (7)$$

$$p_\theta(\theta) = \frac{1}{2\pi}, \qquad 0 \leq \theta \leq 2\pi. \quad (8)$$

R_o corresponds to the closest distance the mobile can be from the BS antenna, and is approximately equal to 20 m for microcellular systems and 80 m for macrocellular systems. Note that we do not use mobility correlation statistics in this model because they do not affect the adaptive model (instantaneous adaptation) and its corresponding ASE.

III. Area Spectral Efficiency

In this section, we introduce the concept of area spectral efficiency for fully loaded systems in which the cell's resource (serviced channels) are fully used and the number of interferers is constant and equal to N_I. We generalize the ASE to partially loaded systems in Section VIII.

Define the *reuse distance* D [m] to be the distance between two BS's using the same set of frequencies. The ASE of a cell is defined as the sum of the maximum bit rates/Hz/unit area supported by a cell's BS. Since frequencies are reused at a distance D, the area covered by one of these partitions is roughly $\pi(D/2)^2$ [m^2]. The ASE, A_e [b/s/Hz/m^2], is therefore

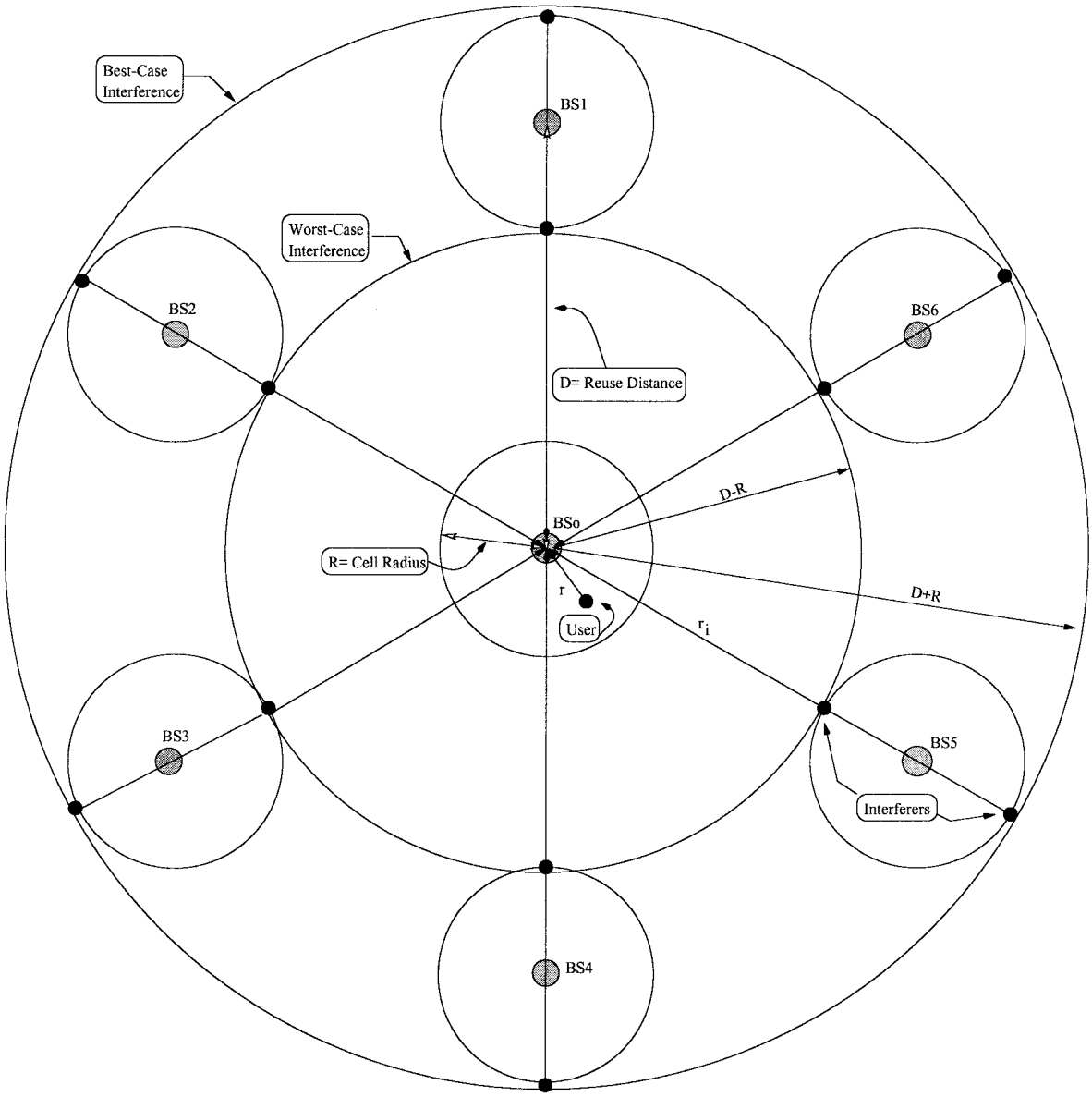

Fig. 1. Cochannel interference on the uplink at a desired BS. In fully loaded nonsectorized cellular systems, there are six primary cochannel interfering mobiles.

approximated by

$$A_e = \frac{\sum_{k=1}^{N_s} C_k}{\pi W (D/2)^2} \tag{9}$$

where N_s is the total number of active serviced channels per cell, C_k [b/s] is the maximum data rate of the kth user, and W [Hz] is the total allocated bandwidth per cell. We define the maximum rate C_k to be the Shannon capacity of the kth user in the cell, which depends on γ_k, the received CIR of that user, and W_k, the bandwidth allocated to that user. The Shannon capacity formula assumes that the interference has Gaussian characteristics. With FDMA or TDMA, there is usually only a few dominant interferers coming from the first ring of interfering cells, so the central limit theorem does not apply and the Gaussian assumption for the interference signal may not be valid. However, for capacity calculations, Gaussian interference is a **worst case** noise assumption [31], [32], and under this assumption the capacity-achieving transmit spectrum for all users (i.e., desired and interfering users) is Gaussian [33]. In addition, the Shannon's formula indicates an arbitrarily small BER, so our ASE is not parameterized by BER. The ASE thus quantifies the tradeoff between the increased system efficiency induced by a small frequency reuse and the decreased capacity of each user resulting from the corresponding increase in cochannel interference. In particular, if we shrink the reuse distance then the denominator of (9) is reduced. However, decreasing the reuse distance increases intercell interference, thereby reducing the CIR of each user, and its corresponding channel capacity. Therefore, there should be an optimal reuse distance which maximizes (9).

For γ_k constant, C_k is given by Shannon's formula: $C_k = W_k \log(1+\gamma_k)$. However, γ_k is not constant in our system since both the interference and signal power of the kth user will vary with mobiles locations and propagation conditions. When γ_k varies with time, C_k equals the average channel capacity of the kth user [34], [35], given by

$$\overline{C}_k = W_k \int_0^{+\infty} \log_2(1+\gamma_k) p_{\gamma_k}(\gamma_k)\, d\gamma_k \tag{10}$$

where $p_{\gamma_k}(\gamma_k)$ is the PDF of the kth user's CIR. The average capacity intrinsically assumes that the users' rate is continuously adapted relative to their CIR (i.e., interference conditions) in such a manner that the BER goes to zero asymptotically. We therefore define the *average area spectral efficiency* $\overline{A}_e$ [b/s/Hz/m^2] as the sum of the maximum average data rates/Hz/unit area for the system, given by (9), with C_k replaced by $\overline{C}_k$. In (10) assuming that all users are assigned the same bandwidth, $\overline{C}_k (=\overline{C})$ becomes the same for all users, and $\overline{A}_e$ can therefore be written as

$$\overline{A}_e = \frac{4N_s\overline{C}}{\pi W R_u^2 R^2} \tag{11}$$

where R_u is the *normalized reuse distance*, $R_u = D/R$.

Consider first FDMA systems, where all users are allocated the same bandwidth $W_k = W_o = W/N_s$. Substituting in (11) yields

$$\overline{A}_e^{\mathrm{FDMA}} = \frac{4}{\pi R_u^2 R^2} \int_0^{+\infty} \log_2(1+\gamma) p_\gamma(\gamma)\, d\gamma. \tag{12}$$

In TDMA systems, the total bandwidth is allocated to only one active user per time slot ($N = 1$ and $W_k = W$). Substituting this in (11) we see that TDMA systems have the same ASE as FDMA systems, so

$$\overline{A}_e^{\mathrm{FDMA}} = \overline{A}_e^{\mathrm{TDMA}} = \overline{A}_e. \tag{13}$$

IV. Effect of Path Loss

In this section, we study the ASE of fully loaded systems, ignoring the effects of shadowing and multipath fading. We obtain the reuse distance which maximizes the ASE and also determine the impact of the cell size, carrier frequency, propagation parameters, and cell sectorization.

A. Analyses

Recall that due to the random location of users in their respective cells, γ_d is a random variable depending on the random positions of the (N_I+1) desired and interfering mobiles. To simplify our analysis, we reduce the problem from (N_I+1) dimensions to one dimension by computing γ_d and the corresponding ASE for the worst case ($-$) and best case ($+$) interference configurations. Without power control, the worst case interference configuration corresponds to the case where all the N_I cochannel interferers are on the near boundary of their respective cells, at a distance $r_I^- = D - R$ [m] from the desired mobile's BS. On the other hand, the best case interference configuration corresponds to the case where all the N_I cochannel interferers are on the far boundary of their cells, at a distance $r_I^+ = D + R$ [m] from this BS. The worst case and the best case interference configurations are illustrated in Fig. 1. Assuming that the transmitted power of all users is the same and substituting (1) into (6) yields

$$\overline{\gamma}_d^{\pm}(N_I, r) = \frac{S_d}{\left(\sum_{i=1}^{N_I} S_i\right)^{\pm}} = \frac{1}{N_I}\left[\frac{R(R_u \pm 1)}{r}\right]^a \left[\frac{g + (R_u \pm 1)R}{g+r}\right]^b. \tag{14}$$

Note that γ_d is function of r, so the desired user capacity is

$$\overline{C}^{\pm}(N_I, r) = W_o \log_2(1 + \overline{\gamma}_d^{\pm}(N_I, r)) \tag{15}$$

for γ_d given by (14). Substituting (15) in (11) yields the ASE conditioned on the desired mobile position r, for a fully loaded system. Integrating (15) over the desired user's position PDF (7) yields the average ASE for the two extreme interference configurations as

$$\langle \overline{A}_e(N_I) \rangle^{\pm} = \frac{4}{\pi R_u^2 R^2} \int_{R_o}^{R} \log_2\left(1 + \overline{\gamma}_d^{\pm}(N_I, r)\right) p_r(r)\, dr. \tag{16}$$

In (16) and in what follows, the brackets denotes the operation of averaging over the desired user's position PDF (7). In practice, when each interferer i is uniformly distributed at a distance r_i between r_I^- and r_I^+, the average ASE will be between these bounding values, as we will confirm by Monte Carlo simulations.

B. Monte Carlo Simulations

The exact analytical value of $\langle \overline{A}_e \rangle$, averaged over the random positions of the desired and interfering users, requires a numerical (N_I+1)-fold integration, which is not only computationally burdensome but also subject to roundoff and stability problems. Rather than computing this integral, we instead opted for a Monte Carlo simulation to estimate it. The simulation algorithm is composed of the following steps.

1) The position of the desired user is randomly picked according to (7) as follows.
   a) Generate a pseudorandom number u uniformly distributed in [0, 1].
   b) Deduce the user's position r according to (7) using the percentile transformation method [36, p. 226]
   $$r = R_o + (R - R_o)\sqrt{u}. \tag{17}$$
2) The polar coordinates (x_i, θ_i) of the N_I cochannel interferers are randomly picked according to (7) and (8) as follows.
   a) Generate N_I pseudorandom, pseudoindependent numbers u_i and v_i uniformly distributed in [0, 1].
   b) Deduce the N_I polar coordinates (x_i, θ_i) as
   $$x_i = R_o + (R - R_o)\sqrt{u_i} \tag{18}$$
   $$\theta_i = 2\pi v_i. \tag{19}$$

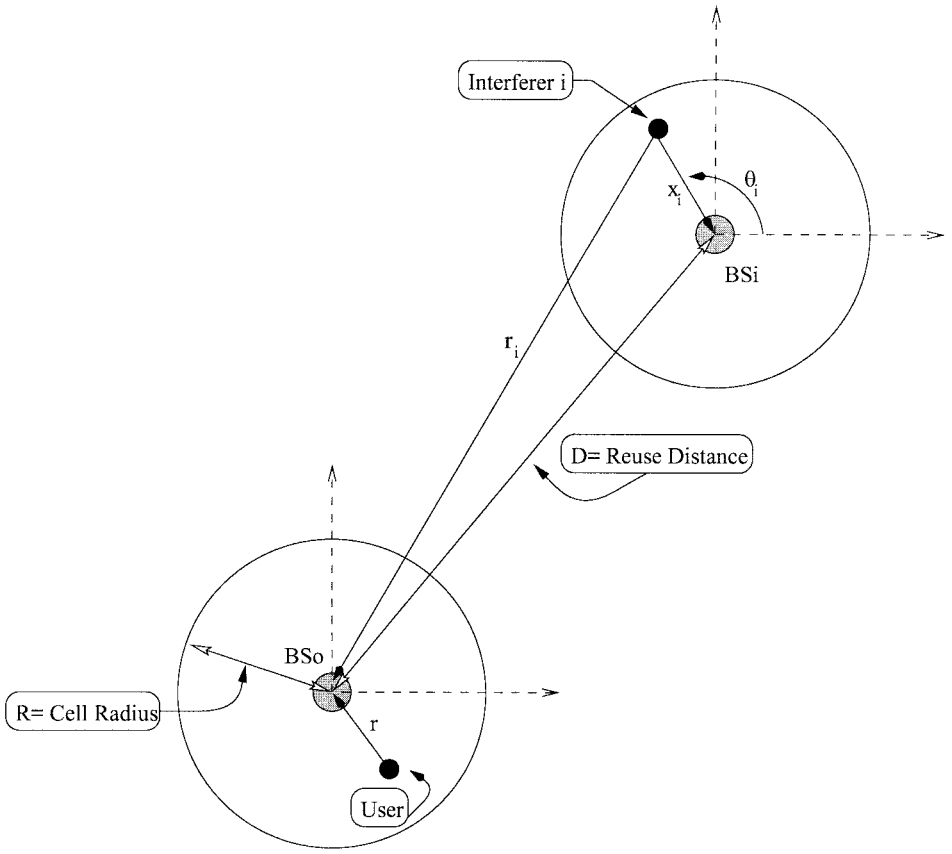

Fig. 2. Geometry of the problem.

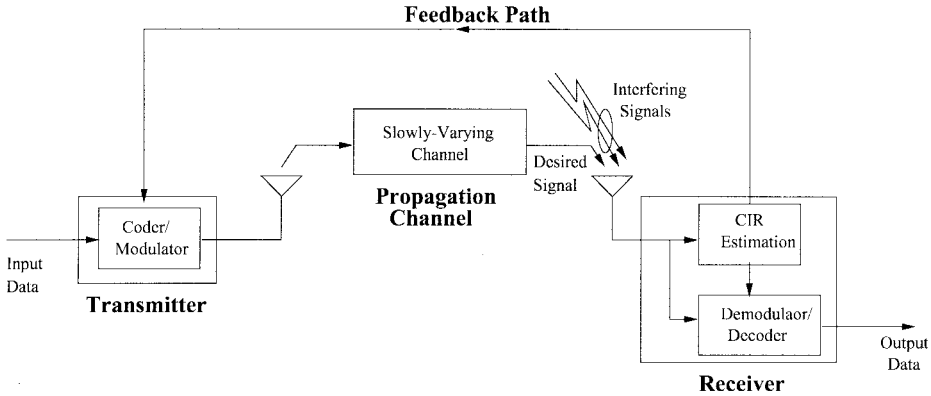

Fig. 3. Adaptive transmission system model (CIR).

3) The distance r_i from each cochannel interferer to the considered BS is calculated as (see Fig. 2)

$$r_i = \sqrt{D^2 + x_i^2 + 2Dx_i \sin(\theta_i)}. \tag{20}$$

4) The N_I+1 average received signal power of the desired user and interfering mobiles ($\overline{S}_d$ and $\overline{S}_i$'s) are calculated using the two-slope path model (1).
5) The CIR of the desired user γ_d is then obtained according to (6).
6) The ASE A_e is calculated as

$$\overline{A}_e = \frac{4}{\pi R_u^2 R^2} \log_2(1+\gamma_d). \tag{21}$$

Repeating the above process [steps 1)–6)] 10 000 times, we can estimate the value of $\langle \overline{A}_e \rangle$ by taking the average of all the observations of the ASE as given by (21). After 10 000 computations, $\langle \overline{A}_e \rangle$ converges to within a three-digit accuracy.

C. Numerical and Simulation Results

In this section, we compute the effects of propagation parameters, the cell size, and carrier frequency on the ASE of fully loaded cellular systems. The ASE for the worst case ($\langle A_e \rangle^-$) and the best case ($\langle A_e \rangle^+$) interference configurations are numerically computed for specific system parameters. Based on the Monte Carlo simulation described in

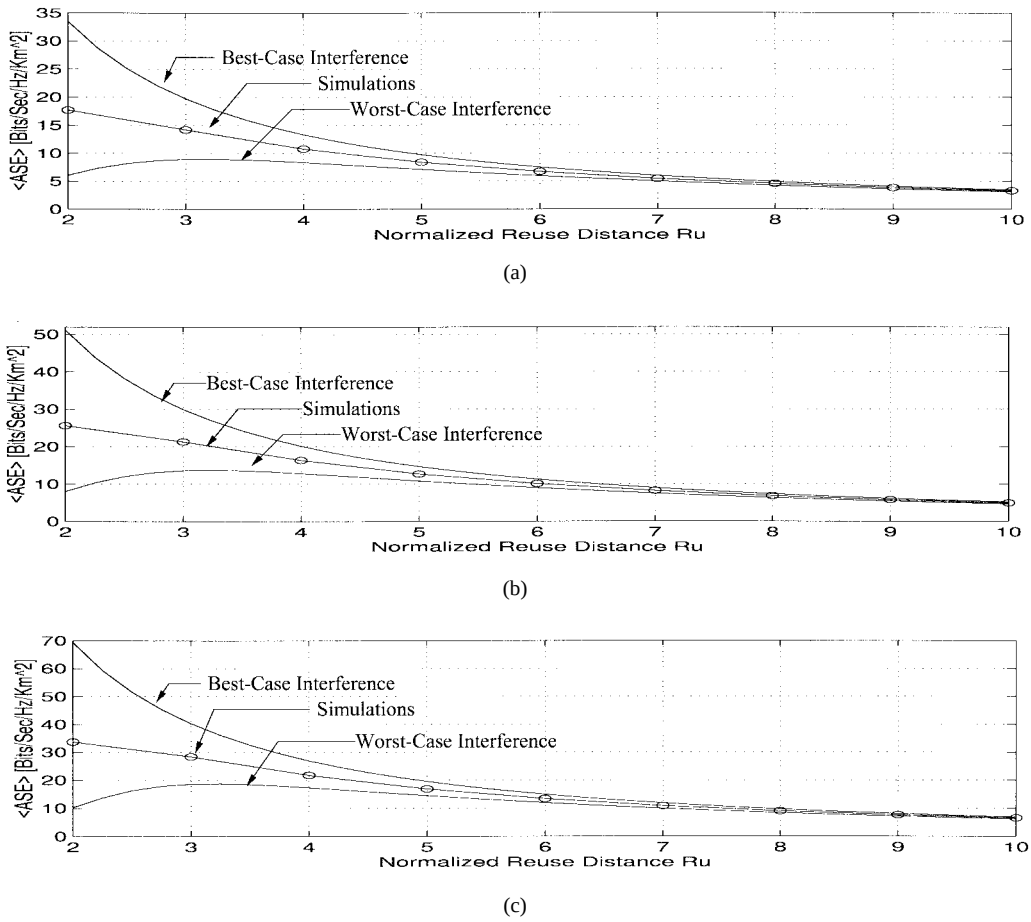

Fig. 4. Comparison of the average uplink area spectral efficiency versus the normalized reuse distance for different values of the additional path exponent b. (Fully loaded system with $N_I = 6$; cell radius $R = 200$ m; $R_o = 20$ m; antenna heights: 10-m BS, 2-m mobile; carrier frequency $f_c = 900$ MHz; basic path exponent: $a = 2$.) (a) $b = 2$, (b) $b = 4$, and (c) $b = 6$.

Section IV-B, the exact value of $\langle A_e \rangle$ is also estimated for the same system parameters of interest.

Fig. 4 depicts the effect of path-loss propagation parameters on the ASE. Our computer simulations confirm our analysis, since the simulated values always lie between the predicted theoretical bounds corresponding to the two extreme interference configurations. As expected the spectral efficiency improves as the additional path-loss exponent b increases, since the interfering signals are more attenuated.

Fig. 5 shows plots of the ASE versus the normalized reuse distance for typical microcellular systems [(a) $R = 200$ m and (b) $R = 800$ m] and macrocellular systems [(c) $R = 5$ km]. We see from this figure that the spectral efficiency is increased by decreasing the cell size. This observation is further investigated in Fig. 6, where we plot the ASE as a function of the cell radius. The "○" points in Fig. 6 correspond to simulation results, whereas the curves correspond to the best fit in the mean-square-error sense of these simulated values. We found that the ASE decreases as an exponential of a fourth-order polynomial relative to the cell size. Thus, we have exactly quantified how spectral efficiency of cellular systems increases as cell size decreases.

Figs. 4 and 5 both indicate that, based on the worst case interference configuration curves, the optimal reuse distance to maximize the ASE is four. In fact, the actual optimum occurs for a reuse distance of about three. However, our statement is based on the fact that R_u is constrained, by definition, to be an even number. On the other hand, the best case interference configuration and the average interference configuration (simulation) curves do not show an ASE maximum. This implies that, for typical interference conditions, the spectral efficiency is maximized by a reuse distance of two (i.e., frequencies are reused every cell), and is monotonically decreasing for $R_u \geq 2$. Note that because our ASE is defined in terms of Shannon capacity, this increase in spectral efficiency is not obtained at the expense of a higher BER. In fact, smaller frequency reuse results in a higher BER only if the data rate of the system is not adapted to compensate for the resulting higher level of cochannel interference [4], [5], [8]. We will see in the following sections that all these results still hold when shadowing and fading are taken into account.

The ASE is increased if interference can be reduced while maintaining the same number of users per cell and the same reuse distance. Cell sectorization [37] is commonly employed to accomplish this, whereby directional antennas are used at the BS. In fully loaded systems, three-sector antennas (or 120° cell sectorization) reduces the number of primary cochannel interferers from $N_I = 6$ to $N_I = 2$. Fig. 7 shows the improvement in ASE when a 120° cell sectorization is employed for a $R = 200$ m microcellular system. Note the

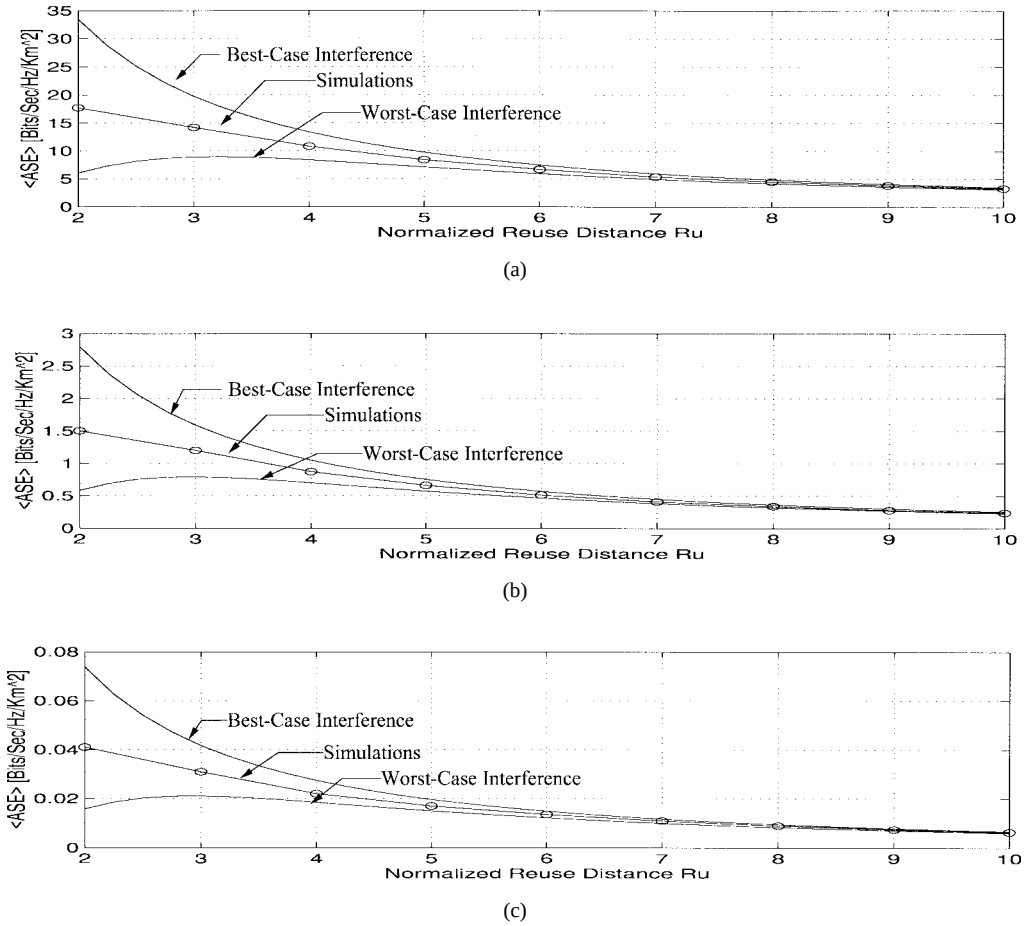

Fig. 5. Comparison of the average uplink area spectral efficiency versus the normalized reuse distance for different cell sizes. (Fully loaded system with $N_I = 6$; carrier frequency $f_c = 900$ MHz; propagation parameters: $a = b = 2$.) (a) $R = 200$ m, (b) $R = 800$ m, and (c) $R = 5$ km.

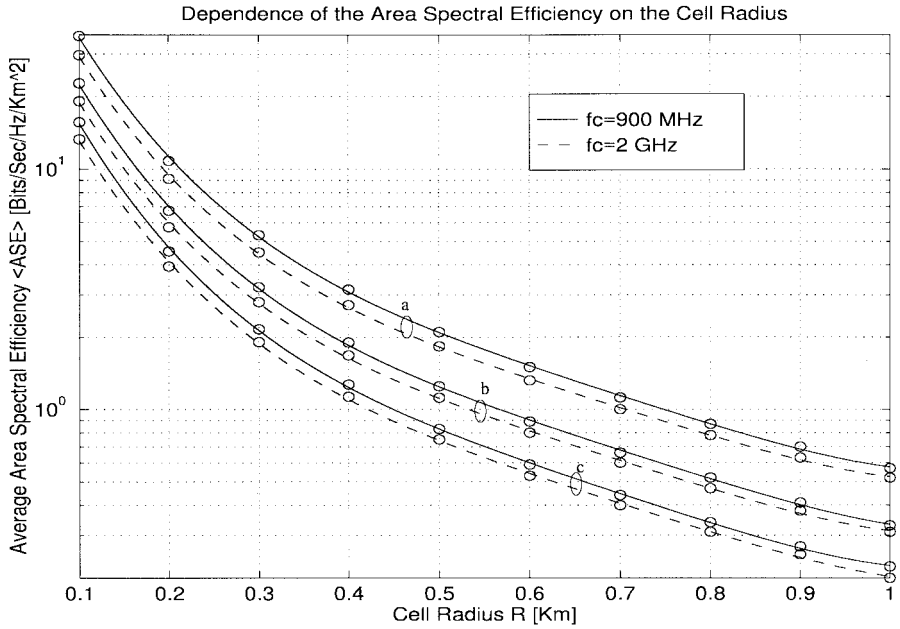

Fig. 6. Average uplink area spectral efficiency versus cell radius for different reuse distances [(a) $R_u = 4$, (b) $R_u = 6$, and (c) $R_u = 8$] and carrier frequencies [(−) $f_c = 900$ MHz and (− −) $f_c = 2$ GHz]. (Fully loaded system with $N_I = 6$; $R_o = 20$ m; antenna heights: 10-m BS, 2-m mobile; propagation parameters: $a = b = 2$.)

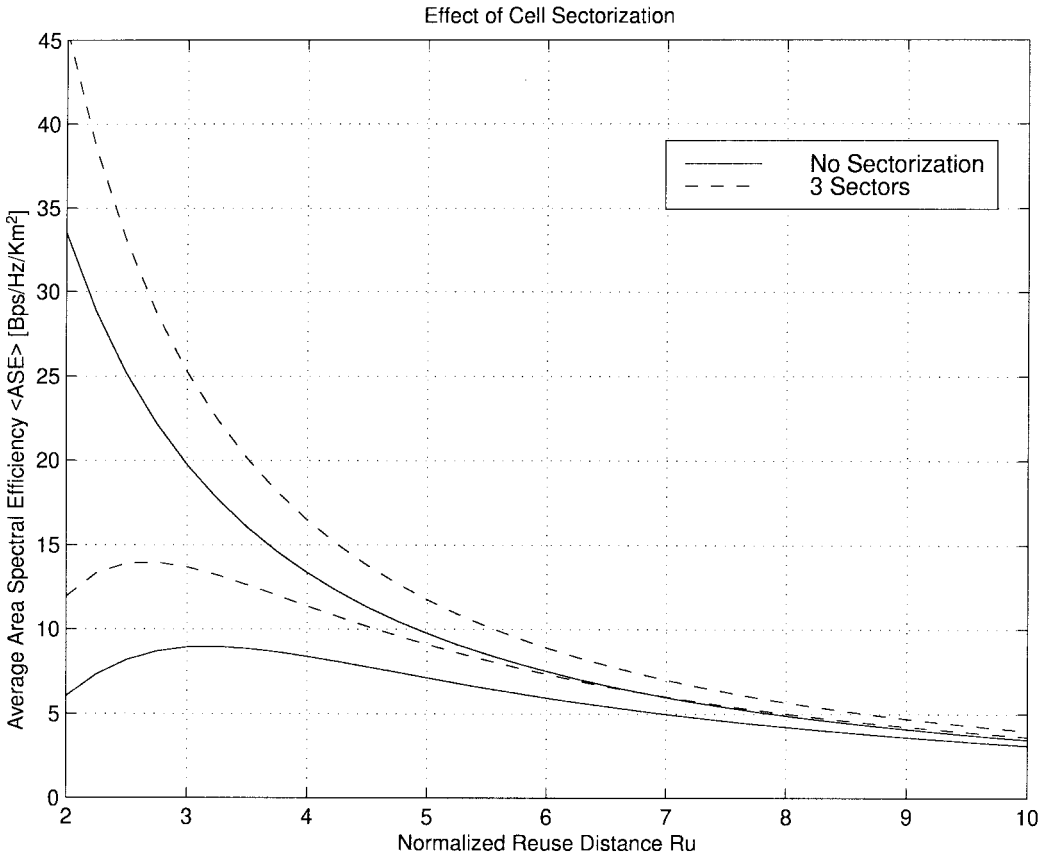

Fig. 7. Average uplink area spectral efficiency versus normalized reuse distance with 120° cell sectorization. (Fully loaded system with $N_I = 6$; cell radius $R = 200$ m; $R_o = 20$ m; antenna heights: 10-m BS, 2-m mobile; carrier frequency $f_c = 900$ MHz; propagation parameters: $a = b = 2$.)

ASE increase in both the upper and lower dashed curves compared to the omnidirectional case (solid curves). Further improvement on the ASE can be obtained with 60° cell sectorization (six-sector antennas) since the number of primary cochannel interferers is reduced in that case to $N_I = 1$.

V. Effect of Shadowing

In this section, we consider the ASE of a fully loaded cellular system when both the desired and interfering users are affected by lognormal shadowing superimposed on path loss. This case applies when the BS radio receiver is able to average out the fast multipath fading, in which case the adaptive system need only react to lognormal channel variations. This is also the scenario when an efficient antenna diversity-combining system is used at the BS to eliminate the effects of multipath fading.

A. Analyses

The desired user's signal is assumed to be lognormally shadowed according to (2) with area mean power μ_d and standard deviation σ_d. There are N_I mutually independent lognormally shadowed interferers, each with mean μ_i and standard deviation σ_i. The interferers are assumed to be statistically identical so that

$$\mu_i = \mu_I, \qquad i = 1, 2, \cdots, N_I \tag{22}$$

$$\sigma_i = \sigma_I, \qquad i = 1, 2, \cdots, N_I. \tag{23}$$

We will refer to all these assumptions from now on as the independent identically distributed (i.i.d.) hypothesis on the $S_i s$. Assumptions (22) and (23) hold when all the N_I interferers are constrained to be on a circle of radius r_I from the considered BS. Note that these assumptions are not essential in our derivation of the ASE. Our analyses can be easily generalized for interferers which are not i.i.d., but this assumption makes our analyses more tractable.

1) PDF of the Desired User CIR: The total interference power S_I is the sum of N_I i.i.d. lognormally distributed RV's. Although no exact closed-form expression for the PDF of the sum of lognormally distributed RV's is known, it is widely accepted that such a sum can be accurately approximated by another lognormal distribution [22, Sec. 3.1]. Several methods have been proposed to find the mean and variance of the resulting lognormal PDF [38], [39]. A very thorough description and comparison of these methods is available in [22, Sec. 3.1]. Here, we use the Fenton–Wilkinson method [38] for its relative simplicity. According to this method, the logarithmic mean μ_{S_I} and the logarithmic variance σ_{S_I} of S_I can be found by matching the first- and second-order moments, which yields

$$\mu_{S_I} = \mu_I + \xi \ln(N_I) + \frac{\sigma_I^2}{2\xi} - \frac{\xi}{2} \ln\left(\frac{N_I - 1 + e^{\sigma_I^2/\xi^2}}{N_I}\right) \tag{24}$$

$$\sigma_{S_I}^2 = \xi^2 \ln\left(\frac{N_I - 1 + e^{\sigma_I^2/\xi^2}}{N_I}\right). \tag{25}$$

Since the ratio of two lognormal RV's is also a lognormal RV, the desired user CIR, γ_d, is also lognormally distributed with the following logarithmic mean μ_{γ_d} and logarithmic variance $\sigma_{\gamma_d}^2$:

$$\mu_{\gamma_d} = \mu_d - \mu_{S_I} \tag{26}$$

$$\sigma_{\gamma d}^2 = \sigma_d^2 + \sigma_{S_I}^2. \tag{27}$$

The PDF of γ_d can therefore be written as

$$p_{\gamma_d}(\gamma) = \frac{\xi}{\sqrt{2\pi}\sigma_{\gamma_d}\gamma} \exp\left(-\frac{(\xi \ln(\gamma) - \mu_{\gamma_d})^2}{2{\sigma_{\gamma_d}}^2}\right), \quad \gamma \geq 0. \tag{28}$$

2) Desired User Average Capacity: Inserting (28) in (10), the average capacity of the desired user can be written as

$$\overline{C} = \frac{W_o \log_2(e)\xi}{\sqrt{2\pi}\sigma_{\gamma_d}} \int_0^{+\infty} \frac{\ln(1+\gamma)}{\gamma} \cdot \exp\left(-\frac{(\xi \ln(\gamma) - \mu_{\gamma_d})^2}{2{\sigma_{\gamma_d}}^2}\right) d\gamma_d. \tag{29}$$

Using the following inequality in (29):

$$\ln(1+\gamma) \leq \ln(\gamma) + \frac{1}{\gamma}, \qquad \gamma \geq 0 \tag{30}$$

we obtain an upper bound on the desired user average capacity $\overline{C}_{\text{up}}$ given by

$$\overline{C} \leq \overline{C}_{\text{up}} = W_o \log_e(e)\left[\frac{\mu_{\gamma_d}}{\xi} + \exp\left(-\frac{\mu_{\gamma_d}}{\xi} + \frac{\sigma_{\gamma_d}^2}{2\xi^2}\right)\right]. \tag{31}$$

On the other hand, using the following inequalities in (29):

$$\ln(1+\gamma) \geq \ln(\gamma) + \frac{1}{1+\gamma} \geq \ln(\gamma) + (1-\gamma)P_{[0,1]}(\gamma), \qquad \gamma \geq 0 \tag{32}$$

where $P_{[0,1]}(\gamma) = 1$ when $\gamma \in [0, 1]$ and zero otherwise, we obtain a lower bound on the desired user average capacity $\overline{C}_{\text{low}}$ given by

$$\overline{C} \geq \overline{C}_{\text{low}} = W_o \log_e(e) \cdot \left[\frac{\mu_{\gamma_d}}{\xi} + Q\left(\frac{\mu_{\gamma_d}}{\sigma_{\gamma_d}}\right) - \exp\left(\frac{\mu_{\gamma_d}}{\xi} + \frac{\sigma_{\gamma_d}^2}{2\xi^2}\right) \cdot Q\left(\frac{\mu_{\gamma_d}}{\sigma_{\gamma_d}} + \frac{\sigma_{\gamma_d}}{\xi}\right)\right] \tag{33}$$

where $Q(.)$ is the *Gaussian integral function* defined as

$$Q(z) = \frac{1}{\sqrt{2\pi}} \int_z^{+\infty} e^{-t^2/2}\, dt. \tag{34}$$

3) ASE for the Two Extreme Interference Configurations: Substituting (29) in (11) yields the ASE for the two extreme interference configurations in a shadowing environment as

$$\overline{A}_e^{\pm}(r) = \frac{4\overline{C}^{\pm}(r)}{\pi W_o R_u^2 R^2}. \tag{35}$$

Similarly substituting (31) and (33) in (11) yields an upper and a lower bound on the ASE as given by (35) for the two extreme interference configurations

$$\frac{4\overline{C}_{\text{low}}^{\pm}(r)}{\pi W_o R_u^2 R^2} \leq \overline{A}_e^{\pm}(r) \leq \frac{4\overline{C}_{\text{up}}^{\pm}(r)}{\pi W_o R_u^2 R^2}. \tag{36}$$

Note that $\overline{C}^{\pm}(r)$, $\overline{C}_{\text{up}}^{\pm}(r)$, and $\overline{C}_{\text{low}}^{\pm}(r)$ are computed using

$$\mu_{\gamma_d}^{\pm} = \mu_d - \mu_{S_I}^{\pm} = \xi \ln\left[\left[\frac{R(R_u \pm 1)}{r}\right]^a \left[\frac{g + (R_u \pm 1)R}{g + r}\right]^b\right] - \xi \ln(N_I) + \frac{\sigma_{S_I}^2 - \sigma_I^2}{2\xi} \tag{37}$$

and $\sigma_{\gamma_d}^2$ given by (27). Since the expressions in (35) and (36) are conditioned on the desired mobile position, they are averaged over the user's position PDF (7), to obtain the overall average ASE $\langle \overline{A_e} \rangle^{\pm}$ for the two extreme interference configurations.

B. Numerical and Simulation Results

Fig. 8 compares the closed-form upper and lower bounds (36) averaged over (7) with the exact value $\langle \overline{A}_e \rangle^{\pm}$ found by averaging (35) over (7) with $\sigma_d = \sigma_I = 4$ dB for the two extreme interference configurations. The bounds are very tight for the best case interference configuration. As R_u increases, the bounds become tighter. On the other hand, the bounds are quite loose for the worst interference configuration when $R_u < 3$. This is because the inequalities (30) and (32) are not tight when γ is small. However, the bounds improve as R_u increases and become very tight for $R_u \geq 4$. The "$\circ$" points in Fig. 9 correspond to simulation results obtained using an algorithm similar to the one described in Section IV-B except for step 4), which is changed to incorporate the effects of shadowing. The changes in the simulation algorithm are described in detail in Appendix A-1. Note again that the simulated values corresponding to average interference configurations always lie between the predicted theoretical values for the two extreme interference conditions.

Fig. 9 compares the ASE with and without shadowing. We see in all cases that the ASE curves for different interference configurations have the same relative shape. However, the ASE with shadowing is always smaller. We will see in the next section that multipath fading also reduces the ASE.

VI. Effect of Multipath Fading

In this section, we consider the ASE of fully loaded cellular systems with Nakagami fading superimposed on path loss. Specifically, we study how the ASE is affected by different amount of fading on the desired and interfering users. This is

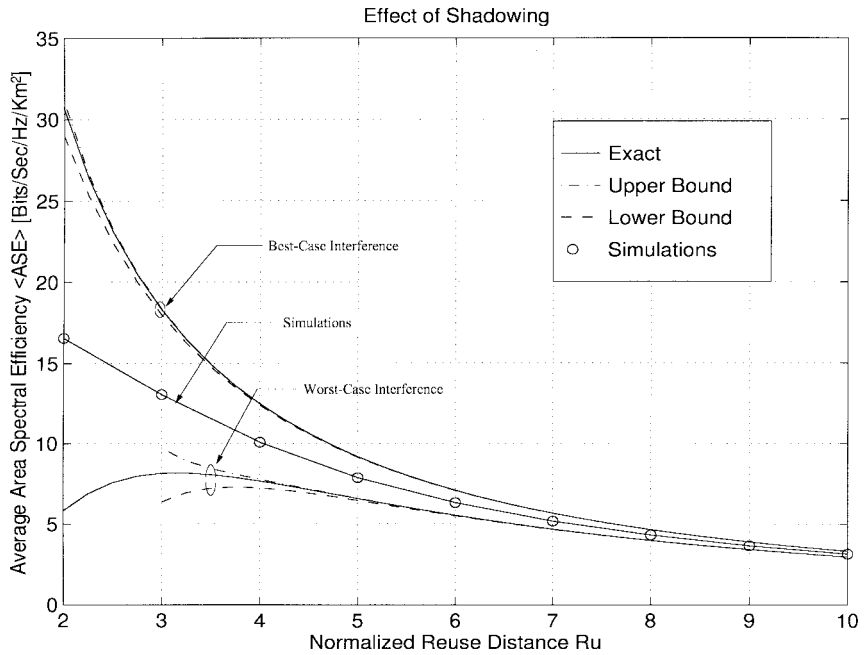

Fig. 8. Comparison of the bounds and the exact values for the average uplink area spectral efficiency with shadowed users ($--$) with $\sigma_d = \sigma_I = 4$ dB. (Fully loaded system with $N_I = 6$; cell radius $R = 200$ m; $R_o = 20$ m; antenna heights: 10-m BS, 2-m mobile; carrier frequency $f_c = 900$ MHz; propagation parameters: $a = b = 2$.)

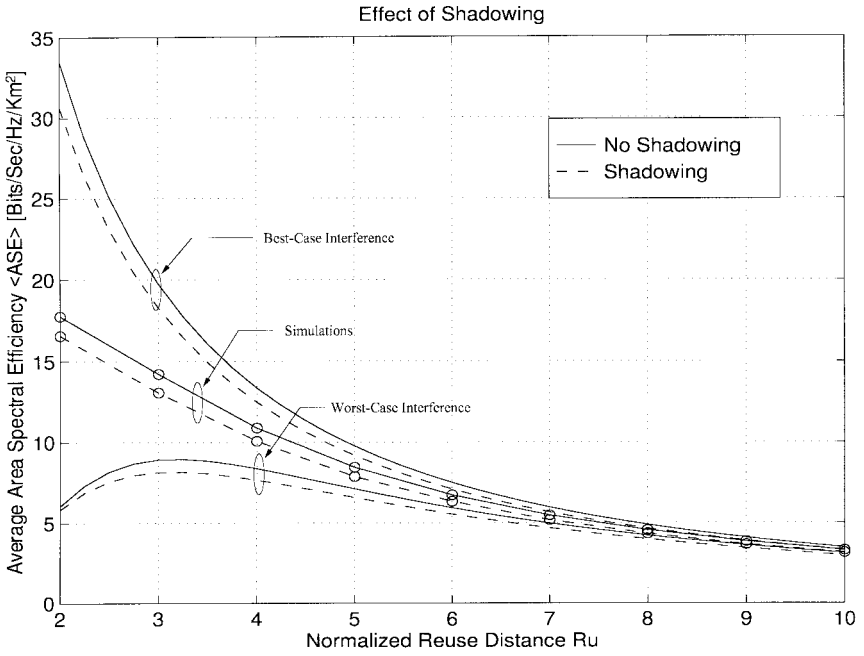

Fig. 9. Comparison of the average uplink area spectral efficiency versus normalized reuse distance with nonshadowed users ($-$) and shadowed users ($--$) with $\sigma_d = \sigma_I = 4$ dB. (Fully loaded system with $N_I = 6$; cell radius $R = 200$ m; $R_o = 20$ m; antenna heights: 10-m BS, 2-m mobile; carrier frequency $f_c = 900$ MHz; propagation parameters: $a = b = 2$.)

of particular interest for microcellular environments in which the desired signal typically experiences less severe fading then the cochannel interfering signals.

A. Analyses

The fading of the desired user's signal has a Nakagami parameter m_d and a local mean power $\overline{S}_d$. There are N_I interferers, each with mutually independent fading, with Nakagami fading parameter m_i and mean power $\overline{S}_i$. The interferers are assumed to be statistically identical so that the S_i's are i.i.d.

$$\overline{S}_i = \overline{S}_I, \qquad i = 1, 2, \cdots, N_I \tag{38}$$

$$m_i = m_I, \qquad i = 1, 2, \cdots, N_I. \tag{39}$$

Assumption (38) holds when all the N_I interferers are constrained to be on a circle of radius r_I from the considered

BS. This assumption is convenient for deriving the ASE in the worst case and best case interference configurations.

1) PDF of the Desired User CIR: Let $\Phi_{S_i}(.)$ denote the characteristic function (CF) of the received power of the ith interferer. As a CF of a gamma RV, $\Phi_{S_i}(.)$ is given by

$$\Phi_{S_i}(\omega) = E(e^{j\omega S_i}) = \frac{1}{(1 - j\omega\overline{S}_I/m_I)^{m_I}}. \quad (40)$$

Since we assume that the S_i are i.i.d., the CF of S_I is just $\Phi_{S_i}(.)$ raised to the power N_I

$$\Phi_{S_I}(\omega) = \frac{1}{(1 - j\omega\overline{S}_I/m_I)^{m_I N_I}}. \quad (41)$$

Thus, N_I Nakagami interferers are equivalent to a single Nakagami interferer with parameter $m_I N_I$ and with local mean power $N_I\overline{S}_I$. Therefore, S_I is gamma distributed with a PDF given by

$$p_{S_I}(s) = \left(\frac{m_I}{\overline{S}_I}\right)^{m_I N_I} \frac{s^{m_I N_I - 1}}{\Gamma(m_I N_I)} \exp\left(-m_I \frac{s}{\overline{S}_I}\right), \quad s \geq 0. \quad (42)$$

Since S_d and S_I are independent, the PDF of γ_d is given by [36, p. 138, eq. (6–43)]

$$p_{\gamma_d}(\gamma) = \int_0^{+\infty} S_I p_{S_d}(\gamma S_I) p_{S_I}(S_I)\, dS_I, \qquad \gamma \geq 0. \quad (43)$$

Substituting (5) and (42) in (43), the PDF of γ_d is found using [24, p. 364, eq. (3.381.4)]

$$p_{\gamma_d}(\gamma) = \left(\frac{m_d}{\overline{S}_d}\right)^{m_d} \left(\frac{m_I}{\overline{S}_I}\right)^{m_I N_I} \cdot \frac{\gamma^{m_d - 1}}{B(m_d, m_I N_I)\left(\frac{m_d}{\overline{S}_d}\gamma + \frac{m_I}{\overline{S}_I}\right)^{m_d + m_I N_I}} \quad (44)$$

where $B(.,.)$ is the *beta function* defined by [24, p. 957, eq. (3.380.1)] as

$$B(p, q) = \int_0^1 t^{p-1}(1-t)^{q-1}\, dt, \qquad p > 0,\ q > 0 \quad (45)$$

and related to the *gamma function* by

$$B(p, q) = \frac{\Gamma(p)\Gamma(q)}{\Gamma(p+q)}. \quad (46)$$

Defining the parameters $\rho = m_d + m_I N_I$ and $y = (m_I\overline{S}_d/m_d\overline{S}_I)$, we can rewrite (44) in a more compact form as

$$p_{\gamma_d}(\gamma) = \frac{y^{\rho - m_d}\gamma^{m_d - 1}(\gamma + y)^{-\rho}}{B(m_d, \rho - m_d)}. \quad (47)$$

Note that for the special case where m_d and m_I are restricted to be positive integers, $p_{\gamma_d}(\gamma)$ reduces to

$$p_{\gamma_d}(\gamma) = \frac{(\rho - 1)!}{(\rho - m_d - 1)!} y^{\rho - m_d}\gamma^{m_d - 1}(\gamma + y)^{-\rho}. \quad (48)$$

2) Desired User Average Capacity: Inserting (48) in (10), the average capacity of the desired user can be written as

$$\overline{C} = \frac{W_o \log_2(e) y^{\rho - m_d}}{B(m_d, \rho - m_d)} \int_0^{+\infty} \frac{\gamma^{m_d - 1} \ln(1 + \gamma)}{(\gamma + y)^{\rho}}\, d\gamma. \quad (49)$$

The integral in (49) can be viewed as the *ρth-order generalized Stieltjes transform* (GST) [40, p. 213], $\mathcal{G}_\rho\{f_{m_d}(.); y\}$, of the function $f_{m_d}(\gamma) = \gamma^{m_d - 1}\ln(1+\gamma)$. Thus, $\overline{C}$ can be written as

$$\overline{C} = \frac{W_o \log_2(e) y^{\rho - m_d}}{B(m_d, \rho - m_d)} \mathcal{G}_\rho\{f_{m_d}(\gamma); y\}. \quad (50)$$

The GST as well as some of its properties that will be useful in our analyses are reviewed in Appendix B. We restrict ourselves in this section to integer values of m_d, but we do not put any constraint on m_I. The evaluation of $\mathcal{G}_\rho\{f_{m_d}(\gamma); y\}$ is derived in Appendix C and is given in (82). Using that result, we can rewrite $\overline{C}$ as

$$\overline{C} = \frac{W_o \log_2(e) y}{B(m_d, \rho - m_d)} \cdot \left| \sum_{j=0}^{m_d - 1} \frac{(-1)^j \binom{m_d - 1}{j}}{(\rho - j - 1)^2} F(1, 1; \rho - j; 1 - y) \right| \quad (51)$$

where $F(.,.;.;.)$ is the *Gauss' hypergeometric function* defined as [24, p. 1065, eq. (9.100)]

$$F(\alpha, \beta; \gamma; z) = \frac{\Gamma(\gamma)}{\Gamma(\alpha)\Gamma(\beta)} \sum_{j=0}^{+\infty} \frac{\Gamma(\alpha + j)\Gamma(\beta + j)}{\Gamma(\gamma + j)} \cdot \frac{z^j}{j!} \quad (52)$$

and $\binom{n}{k}$ denotes the binomial coefficient.

For the special case of $y = 1$ [i.e., $(\overline{S}_d/m_d) = (\overline{S}_I/m_I)$], using [24, p. 589, eq. (4.293.14)] $\overline{C}$ reduces to

$$\overline{C} = W_o \log_2(e)(\psi(\rho) - \psi(\rho - m_d)) \quad (53)$$

where $\psi(.)$ is the *Euler's psi function* defined by [24, p. 952, eq. (8.360)]

$$\psi(z) = \frac{d}{dz}\ln[\Gamma(z)]. \quad (54)$$

Note that in this special $y = 1$ case, (53) applies even if m_d is not restricted to be an integer [contrary to (51)]. If m_d is restricted to be an integer, we can apply [24, p. 954, eq. (8.365.7)] to (53) to get a very simple expression for $\overline{C}$ as

$$\overline{C} = W_o \log_2(e) \sum_{j=0}^{m_d - 1} \frac{1}{j + m_I N_I}. \quad (55)$$

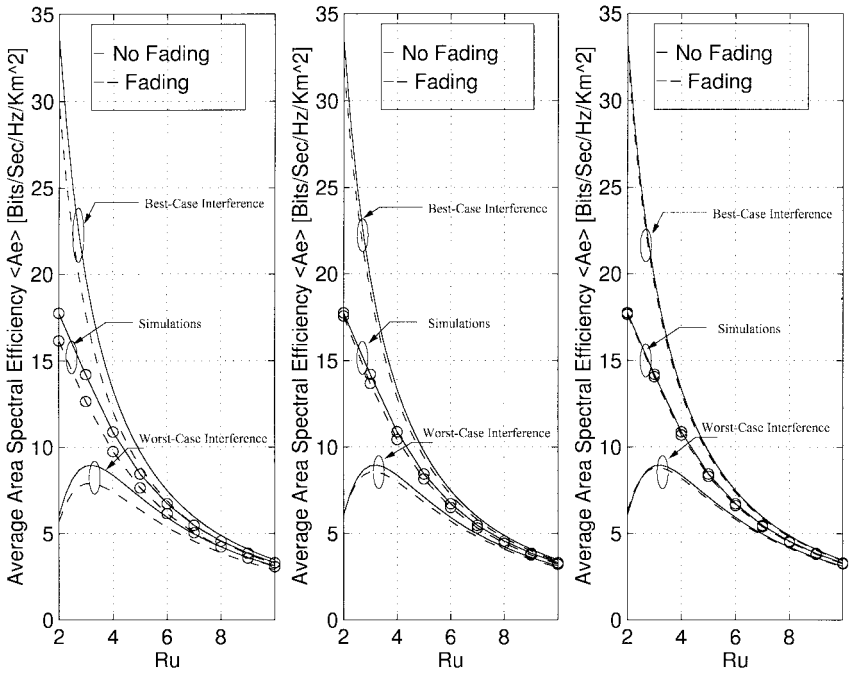

Fig. 10. Effect of the desired users' amount of fading on the average uplink area spectral efficiency. (Fully loaded system with $N_I = 6$; cell radius $R = 200$ m; $R_o = 20$ m; antenna heights: 10-m BS, 2-m mobile; carrier frequency $f_c = 900$ MHz; propagation parameters: $a = b = 2$.) (a) $m_d = 1$; $m_i = 1$, (b) $m_d = 2$; $m_i = 1$, and (c) $m_d = 3$; $m_i = 1$.

3) ASE for the Two Extreme Interference Configurations: Substituting (51) in (11), we get the ASE averaged over the multipath fading and conditioned on the desired mobile position r as

$$\overline{A}_e^{\pm}(r) = \frac{4\log_2(e)y^{\pm}}{\pi B(m_d, m_I N_I)R_u^2 R^2} \cdot \left| \sum_{j=0}^{m_d-1} \frac{(-1)^j \binom{m_d-1}{j}}{(m_d + m_I N_I - j - 1)^2} \cdot F(1, 1; m_d + m_I N_I - j; 1 - y^{\pm}) \right| \quad (56)$$

where

$$y^{\pm} = \frac{m_I}{m_d}\left[\frac{R(R_u \pm 1)}{r}\right]^a \left[\frac{g + (R_u \pm 1)R}{g + r}\right]^b. \quad (57)$$

Integrating (56) over the user's position PDF (7) yields the overall average ASE $\langle \overline{A}_e \rangle^{\pm}$ for the two extreme interference configurations.

B. Numerical and Simulation Results

Figs. 10 and 11 show the ASE for the two extreme interference configuration computed numerically for different values of the Nakagami m fading parameter. These figures also show the exact value of $\langle \overline{A}_e \rangle$ based on a Monte Carlo simulation algorithm using the same system and fading parameters. The simulation algorithm is similar to the one described in Section IV-B except for step 4), which is changed to incorporate the effects of Nakagami fading. The changes in the simulation algorithm are described in detail in Appendix A-2.

First, note again that our computer simulations confirm our analyses, since the simulated values always lie between the predicted theoretical bounds. Comparing these ASE results with our ASE results without fading we see that both sets of ASE curves have the same relative shape, although the ASE with fading is always smaller. Recall that the same behavior was observed for shadowing.

Fig. 10 shows how the desired user's $AF_d = 1/m_d$ affects ASE by fixing $m_I = 1$ (Rayleigh fading) and setting m_d to one [Fig. 10(a)], two [Fig. 10(b)], or three [Fig. 10(c)]. We see that the ASE curves with fading (dashed lines) approach the ASE curves without fading (solid lines) as m_d increases. Hence, as the channel quality between the user and its BS improves (i.e., severity of fading decreases), the system average ASE increases.

Fig. 11 shows how the interferers $AF_I = 1/m_I$ affects the ASE by fixing m_d to be three and setting m_I to one [Fig. 11(a)], two [Fig. 11(b)], or three [Fig. 11(c)]. The interferers' AF seems to have little impact, since the average ASE is about the same (in fact, slightly decreasing with AF_I) for all cases in Fig. 11. Hence, the ASE is predominantly affected by the channel quality of the desired users, rather than by the fading parameters of the interferers.

VII. Combined Effect of Shadowing and Multipath Fading

In this section, we consider the ASE of fully loaded cellular systems in a shadowed/Nakagami fading environment, consist-

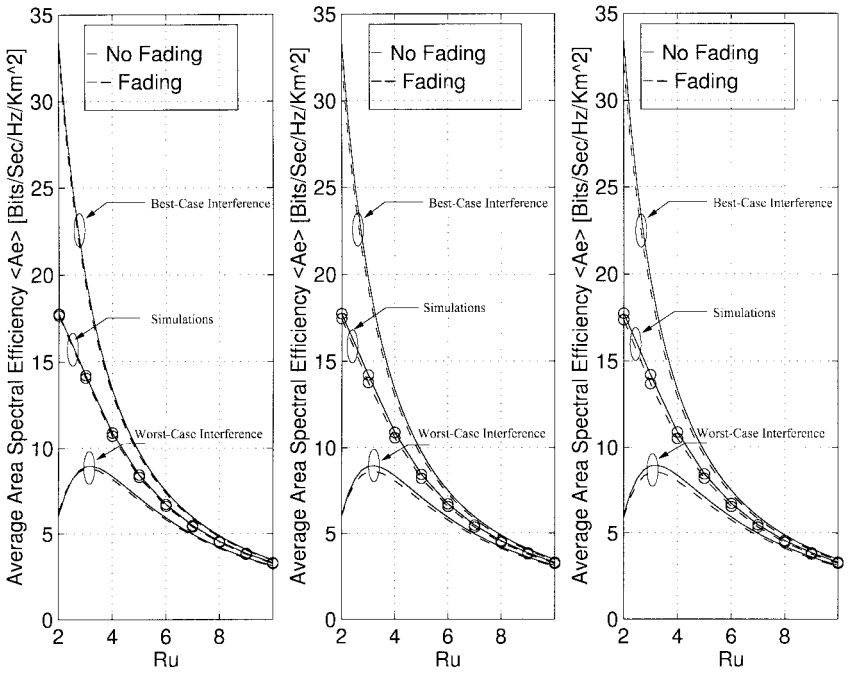

Fig. 11. Effect of the cochannel interferers' amount of fading on the average uplink spectral efficiency. (Fully loaded system with $N_I = 6$; cell radius $R = 200$ m; $R_o = 20$ m; antenna heights: 10-m BS, 2-m mobile; carrier frequency $f_c = 900$ MHz; propagation parameters: $a = b = 2$.) (a) $m_d = 3$; $m_i = 1$, (b) $m_d = 3$; $m_i = 2$, and (c) $m_d = 3$; $m_i = 3$.

ing of Nakagami multipath fading superimposed on lognormal shadowing and two-slope path loss. This is typically the scenario in congested downtown areas with a high number of slow-moving pedestrians and vehicles. Under these conditions, the system does not average out the envelope fading due to multipath, but rather adapts to the instantaneous composite shadowed/faded signal power.

A. Analyses

The desired user's signal is assumed to follow a Nakagami distribution with parameter m_d and a slowly varying local mean power $\overline{S}_d$, which is itself lognormally distributed with area logarithmic mean μ_d and logarithmic standard deviation σ_d. There are N_I i.i.d. Nakagami-faded interferers, each with parameter m_I and a lognormally distributed local mean power $\overline{S}_I$ with area logarithmic mean μ_i and logarithmic variance σ_I.

Combining (2) and (5), we see that the composite shadowed/faded received signal power for all users follows a *gamma/lognormal* PDF given by [22, p. 92, eq. (2.187)]

$$p_S(s) = \int_0^{+\infty} \left(\frac{m}{\overline{S}}\right)^m \frac{s^{m-1}}{\Gamma(m)} \exp\left(-m\frac{s}{\overline{S}}\right) \frac{\xi}{\sqrt{2\pi}\sigma\overline{S}} \cdot \exp\left(-\frac{(\xi \ln \overline{S} - \mu)^2}{2\sigma^2}\right) d\overline{S}. \tag{58}$$

This integral form of the PDF requires numerical techniques for solution and becomes computationally burdensome when further analysis is required. Fortunately, Ho and Stüber [22, p. 92] showed that the composite gamma/lognormal PDF can be accurately approximated by another lognormal PDF with logarithmic mean $\tilde{\mu}$ and logarithmic variance $\tilde{\sigma}^2$. These parameters are obtained by matching the first two moments of (58) with the first two moments of a lognormal approximation giving [22, p. 106]

$$\tilde{\mu} = \xi(\psi(m) - \ln(m)) + \mu \tag{59}$$

$$\tilde{\sigma}^2 = \xi^2\zeta(2, m) + \sigma^2 \tag{60}$$

where $\psi(.)$ is the *Euler's psi function* defined in (54), and $\zeta(.,.)$ is the *generalized Reimann's zeta function* defined by [24, p. 1101, eq. (9.521.1)]

$$\zeta(z, n) = \sum_{j=0}^{+\infty} \frac{1}{(n+j)^z}, \qquad z > 1; n \neq 0, -1, -2, \cdots. \tag{61}$$

Therefore, all the analyses of Section V applies in this case, with the substitution in all the expressions of the μ's by $\tilde{\mu}$'s and the σ^2's by $\tilde{\sigma}^2$'s, for the desired user as well as for the cochannel interferers.

B. Numerical and Simulation Results

The combined effect of shadowing and Nakagami fading on the ASE for the two extreme/average interference configurations is shown in Figs. 12 and 13 with different sets of shadowing and fading parameters. The ASE for the average interference configuration is determined using a simulation algorithm similar to the one used previously except for the generation of the desired (S_d) and interfering (S_i) signal powers, which are obtained as described in Appendix A-3.

Comparing these results with Figs. 10 and 11, we see that the ASE curves still conserve the same relative shape.

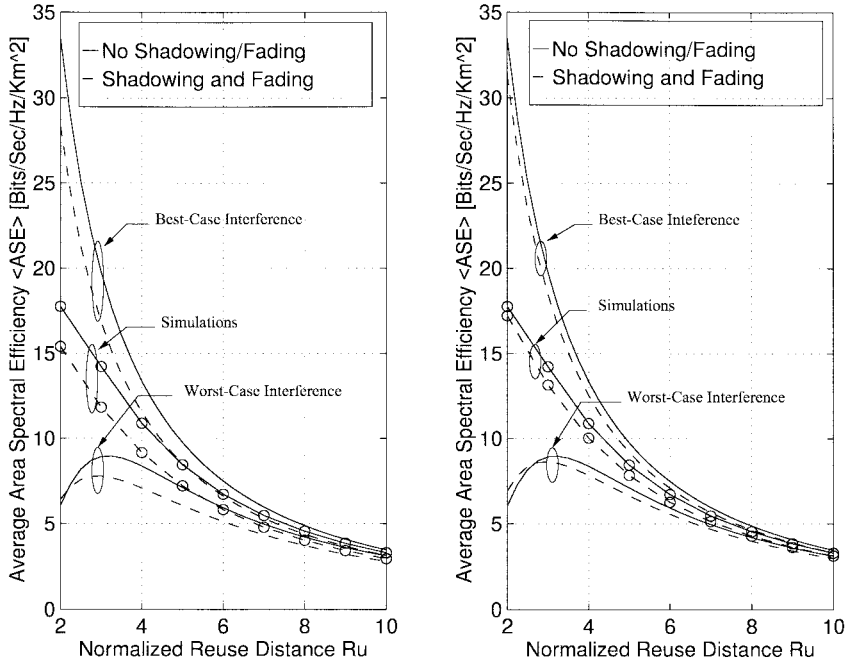

Fig. 12. Combined effect of shadowing ($\sigma_d = \sigma_I = 4$ dB) and Nakagami fading on the average uplink area spectral efficiency. (Fully loaded system with $N_I = 6$; cell radius $R = 200$ m; $R_o = 20$ m; antenna heights: 10-m BS, 2-m mobile; carrier frequency $f_c = 900$ MHz; propagation parameters: $a = b = 2$.) (a) $\sigma = 4$ dB; $m_d = 1$; $m_i = 1$ and (b) $\sigma = 4$ dB; $m_d = 3$; $m_i = 1$.

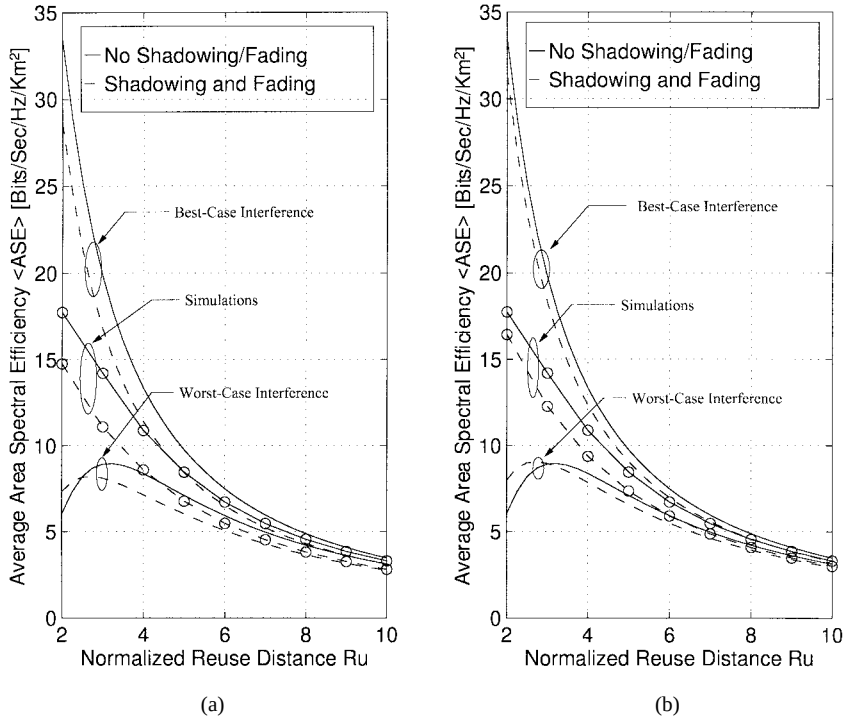

Fig. 13. Combined effect of shadowing ($\sigma_d = \sigma_I = 6$ dB) and Nakagami fading on the average uplink area spectral efficiency. (Fully loaded system with $N_I = 6$; cell radius $R = 200$ m; $R_o = 20$ m; antenna heights: 10-m BS, 2-m mobile; carrier frequency $f_c = 900$ MHz; propagation parameters: $a = b = 2$.) (a) $\sigma = 6$ dB; $m_d = 1$; $m_i = 1$ and (b) $\sigma = 6$ dB; $m_d = 3$; $m_i = 1$.

However, simulations show clearly that for the same amount of multipath fading on the desired and interfering mobiles, shadowing further reduces the system ASE. It is reported in [5], [19], and [39] that the Fenton–Wilkinson method loses its accuracy for $\sigma > 4$ dB and leads to optimistic results for the cochannel interference calculations in that case. This, combined with the fact that the Ho and Stüber approximation increases the shadow standard deviation to incorporate the effect of Nakagami fading (60), explains the slightly high theoretical predictions of the ASE under the combined impact

of shadowing and fading. More accurate ASE predictions can be obtained for high shadow standard deviation if the Schwartz and Yeh's method [39] as reviewed by Prasad and Arnbak [19] is used. This remark also apply for Section V when $\sigma > 4$ dB. Note, however, that all our analyses for Sections V and VII would still apply in that case except that (24) and (25) should be recomputed according to the Schwartz and Yeh's recursive technique [19], [39].

VIII. Partially Loaded Systems

In Section III, we have introduced the ASE for fully loaded cellular systems in which: 1) the cell's serviced channels N_s are all used and 2) the number of interferers is constant and equal to N_I. In this section, we consider partially loaded systems in which the cell's serviced channels and the number of interferers are random variables depending on the traffic loading. In what follows, we first briefly describe a fixed channel assignment scheme. We then study the effect of traffic loading on the ASE when this fixed channel assignment scheme is employed.

A. Channel Assignment Scheme

Each cell has a dedicated and constant number of serviced channels N_s with the same bandwidth $W_o = W/N_s$ [Hz]. In this scheme, if free channels are available in the cell, the BS allocates randomly one of its free channels to a new connection request or handoff attempt. On the other hand, if all serviced channels are busy, any new/handoff connection is blocked or dropped. We assume that the calls are not dynamically ordered/rearranged in order to minimize the number of cochannel interference channels. We also assume that queuing is not provided for connection requests which have been initially blocked or dropped. This channel allocation scheme is obviously quite simple. Besides making our analyses tractable, this schemes offers the advantage of being "instantaneous" (no delay in calls rearrangement), fully distributed, and of very low complexity.

The serviced channels are considered to be independent and active with the same probability p_a. Hence, the blocking/dropping probability B is given by $B = (p_a)^{N_s}$. Equivalently, we have $p_a = B^{1/N_s}$. Thus, the probability that n_s serviced channels are active has a binomial distribution, $P_{n_s}(n_s)$ given by

$$\begin{aligned} P_{n_s}(n_s) &= \binom{N_s}{n_s}(p_a)^{n_s}(1-p_a)^{N_s-n_s} \\ &= \binom{N_s}{n_s}B^{n_s/N_s}(1-B^{1/N_s})^{N_s-n_s}, \\ & \qquad n_s = 0, 1, 2, \cdots, N_s \end{aligned} \tag{62}$$

where $\binom{N_s}{n_s}$ denotes the binomial coefficient.

For a cell with n_s active users, let the number of active cochannel interferes of the kth desired user be denoted by $n_I^{(k)}$, and let $\mathbf{n_I}$ be the vector $[n_I^{(1)}, n_I^{(2)}, \cdots, n_I^{(n_s)}]$. We assume that the $\{n_I^{(k)}\}$ are mutually independent. Hence, the joint distribution of the $\{n_I^{(k)}\}$, $P_{\mathbf{n_I}}(\mathbf{n_I})$, is given by

$$P_{\mathbf{n_I}}(\mathbf{n_I}) = \prod_{k=1}^{n_s} P_{n_I^{(k)}}(n_I^{(k)}). \tag{63}$$

In addition, the $\{n_I^{(k)}\}$ are assumed to be independent from n_s, and the traffic loading conditions are considered to be uniform so that the blocking/dropping probability B is the same for all the cells (desired cell and cochannel interfering cells). Hence, the $\{n_I^{(k)}\}$ are identically distributed according to a binomial distribution $P_{n_I}(n_I)$ given by [3]

$$\begin{aligned} P_{n_I}(n_I) &= \binom{N_I}{n_I}B^{n_I/N_s}(1-B^{1/N_s})^{N_I-n_I}, \\ & \qquad n_I = 0, 1, 2, \cdots, N_I. \end{aligned} \tag{64}$$

B. Analyses

Recall that in partially loaded systems the number of active users n_s and the number of active cochannel interferers $\{n_I^{(k)}\}$ are random variables. Let $\overline{A}_e(n_s, \mathbf{n_I})$ [b/s/Hz/m^2] denote the ASE conditioned on n_s and $\mathbf{n_I}$ and given by

$$\overline{A}_e(n_s, \mathbf{n_I}) = \frac{4}{\pi W R_u^2 R^2}\sum_{k=1}^{n_s}\overline{C}_k(n_I^{(k)}). \tag{65}$$

Averaging (65) over the joint distribution of the $\{n_I^{(k)}\}$, $P_{\mathbf{n_I}}(\mathbf{n_I})$, yields

$$\overline{A}_e(n_s) = \frac{4}{\pi W R_u^2 R^2}\sum_{\mathbf{n_I}}\sum_{k=1}^{n_s}\overline{C}_k(n_I^{(k)})P_{\mathbf{n_I}}(\mathbf{n_I}). \tag{66}$$

Substituting (63) in (66) yields

$$\overline{A}_e(n_s) = \frac{4}{\pi W R_u^2 R^2}\sum_{k=1}^{n_s}\sum_{n_I^{(k)}=0}^{N_I}\overline{C}_k(n_I^{(k)})P_{n_I^{(k)}}(n_I^{(k)}). \tag{67}$$

Using the fact that all users are assigned the same bandwidth, and that the $\{n_I^{(k)}\}$ are independent from n_s and are identically distributed according to $P_{n_I}(n_I)$, (67) simplifies to

$$\overline{A}_e(n_s) = \frac{4n_s}{\pi W R_u^2 R^2}\sum_{n_I=0}^{N_I}\overline{C}(n_I)P_{n_I}(n_I). \tag{68}$$

Averaging (68) over the binomial distribution of n_s (62) yields the average ASE for a partially loaded system as a function of N_s, N_I, and B as

$$\overline{A}_e(N_s, N_I, B) = \frac{4N_sB^{1/N_s}}{\pi W R_u^2 R^2}\sum_{n_I=0}^{N_I}\overline{C}(n_I)P_{n_I}(n_I). \tag{69}$$

Integrating (69) over the user's position PDF (7) yields the overall average ASE, $\langle\overline{A}_e(N_I, N_s, B)\rangle^{\pm}$, for a partially loaded system and for the two extreme configurations. Recall that the traffic loading is directly proportional to the blocking probability B. In the limit of heavy-loaded traffic conditions, $B \to 1$, so that $P_{n_I}(n_I) \to \delta(n_I - N_I)$, where $\delta(k)$ denotes the *Krönecker delta function* which is equal to one for $k = 0$ and zero otherwise. As expected the ASE in this case $\langle\overline{A}_e(N_s, N_I, B)\rangle^{\pm} \overset{B\to 1}{\longrightarrow} \langle\overline{A}_e(N_I)\rangle^{\pm}$, corresponding to the ASE of a fully loaded system.

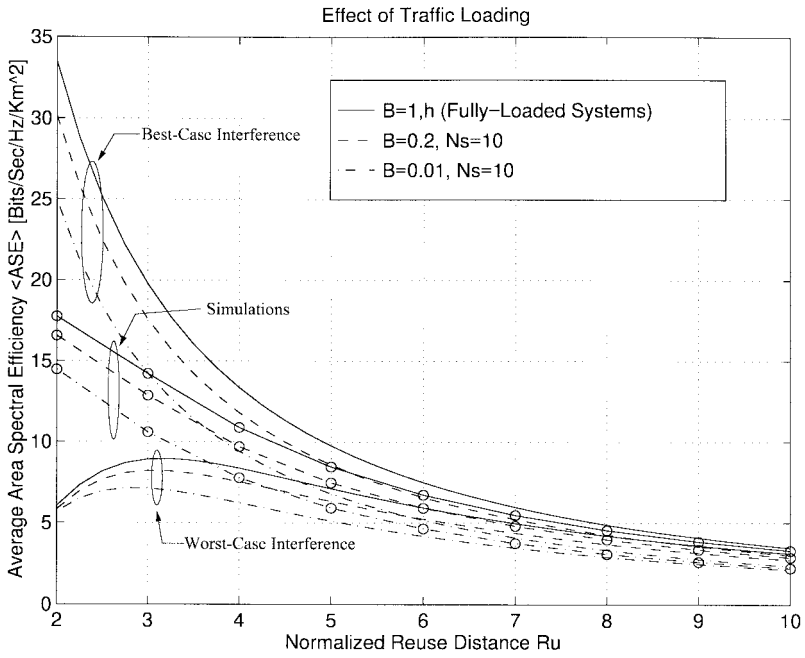

Fig. 14. Comparison of the average uplink area spectral efficiency versus the normalized reuse distance for different traffic loading conditions. (Interferers $N_I = 6$; cell radius $R = 200$ m; $R_o = 20$ m; antenna heights: 10-m BS, 2-m mobile; carrier frequency: 900 MHz; propagation parameters: $a = b = 2$.)

C. Numerical and Simulation Results

The effect of system loading (as parameterized by B) on the ASE for the two extreme/average interference configurations is shown in Fig. 14 for a microcellular radio system with a cell radius $R = 200$ m. Since the effect of shadowing and fading has been thoroughly studied in previous sections, only path loss has been taken into account in computing the desired user average capacity $\overline{C}(n_I)$ in (69). These results can be easily generalized to include the effects of shadowing and fading by recomputing $\overline{C}(n_I)$ in (69) according to (29) and (51), respectively. The "$\circ$" points in Fig. 14 correspond to simulation results obtained using an algorithm similar the one described in Section IV-B except that the number of cochannel interferers n_I is randomly picked following (64). Partially loaded systems have a lower spectral efficiency than fully loaded systems since the ASE increases as the blocking probability increases. Therefore, although the reduced interference to the fewer desired users allows these users to achieve higher rates in partially loaded systems, this effect is more than offset by the fact that with fewer active desired users, only a fraction of the cell allocated bandwidth is used.

IX. Conclusion

We have presented a general analytical framework to quantify the overall spectral efficiency of cellular systems in which mobile users continuously adapt their rate relative to the variation in their respective carrier-to-interference ratio. This efficiency, named the area spectral efficiency, and defined as the sum of the maximum average data rates/unit bandwidth/unit area supported by a cell's base station, captures the tradeoff between a cellular system' spectral efficiency, the link spectral efficiency, and the communication link quality provided to the users. We have calculated this efficiency for FDMA and TDMA systems as a function of the reuse distance for the worst case and best case interference configurations. We have also developed Monte Carlo simulations to estimate the value of this efficiency for average interference conditions. Our theoretical analyses are in good agreement with the corresponding simulated values.

We haven take into account the effect of the users random location in their respective cells and have presented numerical results showing the impact of propagation parameters, cell size, carrier frequency, and cell sectorization on the spectral efficiency. Results indicate that, based on the worst case interference configuration, the optimal reuse distance is approximately four. However, this optimal reuse distance is two for the best case and the average interference configurations (i.e., frequencies should be reused every cell). Moreover, simulation show that area efficiency decreases as an exponential of a fourth-order polynomial relative to the cell size.

We have also studied the area spectral efficiency under the influence of lognormal shadowing and Nakagami multipath fading superimposed on path loss. Results show that both shadowing and fading reduce the area spectral efficiency, but do not affect its general behavior relative to the reuse distance. In addition, the spectral efficiency is predominantly affected by the fading parameters of the desired users, rather than by the fading parameters of the interferers.

This paper also presented initial steps toward the determination of the area spectral efficiency of partially loaded systems. Results reveal that heavier traffic loading (i.e., higher blocking probability) leads to a higher area spectral efficiency when a simple fixed channel allocation scheme. A study with more sophisticated channel allocation schemes is being conducted so as to assess the impact on the area spectral efficiency.

Our results are useful for the prediction of the spectral efficiency of cellular systems with variable-rate transmission under various "realistic" conditions. Furthermore, they provide system engineers with valuable input information for the efficient design, planning, and dimensioning of such systems. In particular, these results give guidelines for optimizing reuse distance and cell size.

APPENDIX A
MONTE CARLO SIMULATIONS

A-1. Shadowing

Step 4) of the algorithm described in Section IV-B is changed as follows to incorporate the effect of shadowing.

- The $N_I + 1$ area mean powers (μ_d and μ_i's) at the considered BS are calculated using the two-slope path model (1).
- The instantaneous received power from the desired and interfering mobiles (S_d and S_i's) are randomly generated according to a lognormal distribution (2) with area means μ_d and μ_i's, respectively, and standard deviations σ_d and σ_I, respectively.

Since we need to average out the additional effect of shadowing a higher number of iterations is required (typically 100 000) than in Section IV-B for the same degree of accuracy in the estimation of $\langle \overline{A}_e \rangle$.

A-2. Multipath Fading

Step 4) of the algorithm described in Section IV-B is changed as follows to incorporate the effect of Nakagami multipath fading.

- The $N_I + 1$ local mean powers ($\overline{S}_d$ and $\overline{S}_i$'s) at the considered BS are calculated using the two-slope path model (1).
- The instantaneous received powers from the desired and interfering mobiles (S_d and S_i's) are randomly generated according to a gamma distribution (5) with fading parameters m_d and m_I, respectively, and local mean powers $\overline{S}_d$ and $\overline{S}_i$'s, respectively.

The same number of iterations as in the shadowing case is typically required to average out the additional effect of multipath and to estimate $\langle \overline{A}_e \rangle$ within a three-digit accuracy.

A-3. Combined Effect of Shadowing and Multipath Fading

Step 4) of the algorithm described in Section IV-B is changed as follows to incorporate the combined effect of shadowing and Nakagami multipath fading.

- The $N_I + 1$ area mean powers (μ_d and μ_i's) at the considered BS are calculated using the two-slope path model (1).
- The slowly varying local mean powers from the desired and interfering mobiles ($\overline{S}_d$ and $\overline{S}_i$'s) are randomly generated according to a lognormal distribution (2) with area means μ_d and μ_i's, respectively, and standard deviations σ_d and σ_I, respectively.
- The instantaneous received power from the desired and interfering mobiles (S_d and S_i's) are randomly generated according to a gamma distribution (5) with fading parameters m_d and m_I, respectively, and local mean powers $\overline{S}_d$ and $\overline{S}_i$'s, respectively.

Since we need to average out the effect of both shadowing and Nakagami fading a higher number of iterations is required (typically 300 000 iterations) than in the previous cases for the same degree of accuracy in the estimation of $\langle \overline{A}_e \rangle$.

APPENDIX B
SOME PROPERTIES OF THE GENERALIZED STIELTJES TRANSFORM (GST)

In this Appendix, we review some basic properties of the GST. We restrict our review to the properties that are useful in our derivation of the ASE in Nakagami fading environment. A more detailed summary of the GST and its properties can be found in [40, ch. XIV].

The GST of order ρ of the function $f(x)$ is defined by

$$\mathcal{G}_\rho\{f(x); y\} = g(y; \rho) = \int_0^{+\infty} f(x)(x+y)^{-\rho}\, dx \quad (70)$$

where y and ρ can be complex variables. The relationship between $g(.; .)$ and $f(.)$ can also be expressed symbolically by a GST transform pair as

$$f(x) \overset{\text{GST}}{\longleftrightarrow} g(y; \rho). \quad (71)$$

Theorem 1—Differentiation Property [40, p. 233, eq. (5)]: Assuming (71) then

$$\frac{d}{dx} f(x) \overset{\text{GST}}{\longleftrightarrow} \rho g(y; \rho + 1) - y^{-\rho} f(0). \quad (72)$$

Theorem 2—Multiplication by x Property [40, p. 233, eq. (2)]: Assuming (71) then

$$x f(x) \overset{\text{GST}}{\longleftrightarrow} g(y; \rho - 1) - y g(y; \rho). \quad (73)$$

Theorem 3—A Useful GST Pair [40, p. 233, eq. (9)]: For $\rho > n - 1$ and assuming (71) then

$$\text{If } f(x) = \frac{x^{n-1}}{1+x}, \quad \text{then}$$
$$g(y; \rho) = \frac{\Gamma(n)\Gamma(1-n+\rho) y^{n-\rho}}{\Gamma(1+\rho)} F(1, n; 1+\rho; 1-y) \quad (74)$$

where $F(., .; .; .)$ is *Gauss' hypergeometric function* defined in (52).

APPENDIX C
EVALUATION OF $\mathcal{G}_\rho\{f_n(x); y\} = g_n(y; \rho)$

In this Appendix, we evaluate the GST of $f_n(x) = x^{n-1} \ln(1+x)$. To simplify our notations, let us denote $\mathcal{G}_\rho\{f_n(x); y\}$ by $g_n(y; \rho)$. First, note that

$$f_1(x) = \ln(1+x) \quad (75)$$

so that

$$\frac{d}{dx}f_1(x) = \frac{1}{1+x}. \tag{76}$$

Using the differentiation property of the GST (72), note that the second term vanishes so that

$$\mathcal{G}_\rho\left\{\frac{d}{dx}f_1(x);\, y\right\} = \rho g_1(y;\, \rho+1). \tag{77}$$

Using the GST transform pair (74) applied (for $n=1$) to (76), then substituting the result in the left-hand side of (77), yields

$$g_1(y;\, \rho) = \frac{y^{2-\rho}}{(\rho-1)^2}F(1,\, 1;\, \rho;\, 1-y) \tag{78}$$

where $F(.,\, .;\, .;\, .)$ is defined in (52). Note that since $\rho = m_d + N_I\, m_I$ and $n = m_d$, we have $\rho - n = N_I m_I > -1$ and therefore (74) always applies with no singularities.

As a second step of our derivation, we apply the property (73) to $f_{n-1}(x)$. This provides a difference equation given by

$$g_n(y;\, \rho) = g_{n-1}(y;\, \rho-1) - y g_{n-1}(y;\, \rho). \tag{79}$$

Then it can be show by induction that for n positive integer

$$g_n(y;\, \rho) = \left|\sum_{j=0}^{n-1}(-1)^j \binom{n-1}{j} g_1(y;\, \rho-j) y^{n-j-1}\right| \tag{80}$$

is solution for the difference equation (79) where $\binom{n-1}{j}$ denotes the binomial coefficient given by

$$\binom{n-1}{j} = \frac{(n-1)!}{j!\,(n-j-1)!}. \tag{81}$$

Finally, inserting (78) in (80), we find $g_n(y;\, \rho)$ as

$$g_n(y;\, \rho) = \left|\sum_{j=0}^{n-1}(-1)^j \binom{n-1}{j} \frac{y^{n-\rho+1}}{(\rho-j-1)^2} \cdot F(1,\, 1;\, \rho-j;\, 1-y)\right|. \tag{82}$$

REFERENCES

[1] K. Pahlavan and A. H. Levesque, "Wireless data communications," *Proc. IEEE*, vol. 82, pp. 1398–1430, Sept. 1994.

[2] V. H. MacDonald, "The cellular concept," *Bell Syst. Tech. J.*, vol. 58, pp. 15–41, Jan. 1979.

[3] R. Muammar and S. C. Gupta, "Cochannel interference in high-capacity mobile radio systems," *IEEE Trans. Commun.*, vol. COM-30, pp. 1973–1978, Aug. 1982.

[4] Y. Nagata and Y. Akaiwa, "Analysis for spectrum efficiency in single cell trunked and cellular mobile radio," *IEEE Trans. Veh. Technol.*, vol. VT-35, pp. 100–113, Aug. 1987.

[5] R. Prasad and A. Kegel, "Improved assessment of interference limits in cellular radio performance," *IEEE Trans. Veh. Technol.*, vol. 40, pp. 412–419, May 1991.

[6] A. A. Abu-Dayya, "Outage probabilities of cellular mobile radio systems with multiple Nakagami interferers," *IEEE Trans. Veh. Technol.*, vol. 40, pp. 757–768, Nov. 1991.

[7] Y.-D. Yao and A. U. H. Sheikh, "Investigations in cochannel interference in microcellular mobile radio systems," *IEEE Trans. Veh. Technol.*, vol. 41, pp. 114–123, May 1992.

[8] R. Prasad and A. Kegel, "Effects of Rician faded and lognormal shadowed signals on spectrum efficiency in microcellular radio," *IEEE Trans. Veh. Technol.*, vol. 42, pp. 274–280, Aug. 1993.

[9] W. T. Webb and L. Hanzo, *Modern Quadrature Amplitude Modulation.* New York: IEEE Press, 1994.

[10] R. Haas and J. Belfiore, "Spectrum efficiency limits in mobile cellular systems," *IEEE Trans. Veh. Technol.*, vol. 45, pp. 33–40, Feb. 1996.

[11] N. Morinaga, M. Yokoyama, and S. Sampei, "Intelligent radio communications techniques for advanced wireless communication systems," *IEICE Trans. Commun.*, vol. E79-B, pp. 214–221, Mar. 1996.

[12] S. M. Alamouti and S. Kallel, "Adaptive trellis-coded multiple-phased-shift keying for Rayleigh fading channels," *IEEE Trans. Commun.*, vol. 42, pp. 2305–2314, June 1994.

[13] T. Ue, S. Sampei, and N. Morinaga, "Symbol rate and modulation level controlled adaptive modulation/TDMA/TDD for personal communication systems," *IEICE Trans. Commun.*, vol. E78-B, pp. 1117–1124, Aug. 1995.

[14] W. T. Webb and R. Steele, "Variable rate QAM for mobile radio," *IEEE Trans. Commun.*, vol. 43, pp. 2223–2230, July 1995.

[15] S. G. Chua and A. Goldsmith, "Variable-rate variable-power M-QAM for fading channels," in *Proc. IEEE Veh. Technol. Conf. VTC'96*, Atlanta, GA, Apr. 1996, pp. 815–819.

[16] H. Matsuoka, S. Sampei, N. Morinaga, and Y. Kamio, "Adaptive modulation system with variable coding rate concatenated code for high quality multi-media communication systems," *IEICE Trans. Commun.*, vol. E79-B, pp. 328–334, Mar. 1996.

[17] D. N. Hatfield, "Measure of spectral efficiency in land mobile radio," *IEEE Trans. Electromagn. Compat.*, vol. EMC-19, pp. 266–268, Aug. 1977.

[18] W. C. Y. Lee, "Spectrum efficiency in cellular," *IEEE Trans. Veh. Technol.*, vol. 38, pp. 69–75, May 1989.

[19] R. Prasad and J. C. Arnbak, "Comments on 'Analysis for spectrum efficiency in single cell trunked and cellular mobile radio,'" *IEEE Trans. Veh. Technol.*, vol. 37, pp. 220–222, Nov. 1988.

[20] P. Harley, "Short distance attenuation measurements at 900 MHz and 1.8 GHz using low antenna heights for microcells," *IEEE J. Select. Areas Commun.*, vol. SAC-7, pp. 5–11, Jan. 1989.

[21] M. V. Clark, V. Erceg, and L. J. Greenstein, "Reuse efficiency in urban microcellular networks," in *Proc. IEEE Veh. Technol. Conf. VTC'96*, Atlanta, GA, Apr. 1996, pp. 421–425.

[22] G. L. Stüber, *Principles of Mobile Communications.* Norwell, MA: Kluwer, 1996.

[23] M. Nakagami, "The m-distribution—A general formula of intensity distribution of rapid fading," in *Statistical Methods in Radio Wave Propagation.* Oxford, U.K.: Pergamon, 1960, pp. 3–36.

[24] I. S. Gradshteyn and I. M. Ryzhik, *Table of Integrals, Series, and Products*, 5th ed. San Diego, CA: Academic, 1994.

[25] U. Charash, "Reception through Nakagami fading multipath channels with random delays," *IEEE Trans. Commun.*, vol. COM-27, pp. 657–670, Apr. 1979.

[26] H. Suzuki, "A statistical model for urban multipath propagation," *IEEE Trans. Commun.*, vol. COM-25, pp. 673–680, July 1977.

[27] T. Aulin, "Characteristics of a digital mobile radio channel," *IEEE Trans. Veh. Technol.*, vol. VT-30, pp. 45–53, May 1981.

[28] A. U. Sheikh, M. Handforth, and M. Abdi, "Indoor mobile radio channel at 946 MHz: Measurements and modeling," in *Proc. Veh. Technol. Conf. VTC'93*, Secaucus, NJ, May 1993, pp. 73–76.

[29] S. A. Abbas and A. U. Sheikh, "On understanding the nature of slow fading in LOS microcellular channels," in *Proc. IEEE Veh. Technol. Conf. VTC'97*, Phoenix, AZ, May 1997, pp. 662–666.

[30] Y. Karasawa and M. Yasunaga, "Interference evaluation method for mobile-satellite systems under Nakagami–Rice fading conditions," *IEICE Trans. Commun.*, vol. E75-B, pp. 42–49, Jan. 1992.

[31] S. Ihara, "On the capacity of channels with additive non-Gaussian noise," *Inform. Control*, vol. 37, pp. 34–39, 1978.

[32] S. Shamai and A. D. Wyner, "Information-theoretic consideration for symmetric cellular, multiple-access fading channels—Part I," *IEEE Trans. Inform. Theory*, vol. 43, pp. 1877–1894, Nov. 1997.

[33] A. Lapidoth, "Nearest neighbor decoding for additive non-Gaussian noise channels," *IEEE Trans. Inform. Theory*, vol. 42, pp. 1520–1529, Sept. 1996.

[34] W. C. Y. Lee, "Estimate of channel capacity in Rayleigh fading environment," *IEEE Trans. Veh. Technol.*, vol. 39, pp. 187–190, Aug. 1990.

[35] C. G. Günther, "Comment on 'Estimate of channel capacity in Rayleigh fading environment,'" *IEEE Trans. Veh. Technol.*, vol. 45, pp. 401–403, May 1996.

[36] A. Papoulis, *Probability, Random Variables, and Stochastic Processes*, 3rd ed. New York: McGraw-Hill, 1991.

[37] G. K. Chan, "Effects of sectorization on the spectrum efficiency of cellular radio systems," *IEEE Trans. Veh. Technol.*, vol. 41, pp. 217–225, Aug. 1992.

[38] L. F. Fenton, "The sum of lognormal probability distributions in scatter transmission systems," *IRE Trans. Commun.*, vol. COM-8, pp. 57–67, Mar. 1960.
[39] S. Schwratz and Y. S. Yeh, "On the distribution function and moments of power sums with lognormal components," *Bell Syst. Tech. J.*, vol. 61, pp. 1441–1462, Sept. 1982.
[40] A. Erdelyi, W. Magnus, F. Oberhettinger, and F. Tricomi, *Table of Integral Transforms.* New York: McGraw-Hill, 1954, vol. 2.

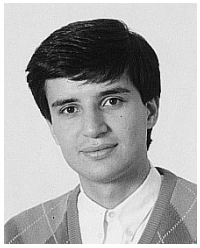

Mohamed-Slim Alouini (S'94–M'99) was born in Tunis, Tunisia. He received the "Diplôme d'Ingénieur" degree from the Ecole Nationale Supérieure des Télécommunications (TELECOM Paris), Paris, France, and the "Diplôme d'Etudes Approfondies (D.E.A.)" degree in electronics from the University of Pierre & Marie Curie (Paris VI), Paris, both in 1993. He received the M.S.E.E. degree from the Georgia Institute of Technology (Georgia Tech), Atlanta, in 1995 and the Ph.D. degree in electrical engineering from the California Institute of Technology (Caltech), Pasadena, in 1998.

While completing his D.E.A. thesis, he worked with the optical submarine systems research group of the French national center of telecommunications (CNET-Paris B) on the development of future transatlantic optical links. While at Georgia Tech, he conducted research in the area of K_a-band satellite channel characterization and modeling. From June 1998 to August 1998, he was a Post-Doctoral Fellow with the Communications Group at Caltech carrying out research on adaptive modulation techniques and on CDMA communications. He joined the Department of Electrical and Computer Engineering, University of Minnesota, Minneapolis, in September 1998, where his current research interests include statistical modeling of multipath fading channels, adaptive modulation techniques, diversity systems, and digital communication over fading channels.

Dr. Alouini is the recipient of a National Semiconductor Graduate Fellowship Award and the Charles Wilts Prize for outstanding independent research in electrical engineering leading to a Ph.D. degree at Caltech. He is a member of the IEEE Communications and Vehicular Technology Societies.

Andrea J. Goldsmith (S'94–M'95) received the B.S., M.S., and Ph.D. degrees in electrical engineering from the University of California, Berkeley, in 1986, 1991, and 1994, respectively.

From 1986 to 1990, she was with Maxim Technologies, where she worked on packet radio and satellite communication systems. From 1991 to 1992, she was with AT&T Bell Laboratories, where she worked on microcell modeling and channel estimation. She was an Assistant Professor of Electrical Engineering at the California Institute of Technology, Pasadena, from 1994 to 1998 and is currently an Assistant Professor of Electrical Engineering at Stanford University, Stanford, CA. Her research includes work in capacity of wireless channels, wireless communication theory, adaptive modulation and coding, joint source and channel coding, and resource allocation in cellular systems.

Dr. Goldsmith is the recipient of the National Science Foundation CAREER Development Award, the ONR Young Investigator Award, two National Semiconductor Faculty Development Awards, an IBM Graduate Fellowship, and the David Griep Memorial Prize from the University California at Berkeley. She is an Editor for the IEEE TRANSACTIONS ON COMMUNICATIONS and the IEEE PERSONAL COMMUNICATIONS MAGAZINE.